- Moore-Ede, M. C., Czeisler, C. A., and Richardson, G. S. 1983 Circadian time-keeping in health and disease Part 2. Clinical implications of circadian rhythmicity. The New England Journal of Medicine 309 (9), 530-534.
- Norman, W. A., and Litwack G. 1997 *Hormones*. 2nd ed. London: Academic Press.
- Orth, D. N. 1992 Corticotropin-releasing hormone in humans. *Endocr. Rev.* 13 (2) 164-191.
- Posener, J. A., Schildkraut, J. J., Williams, G. H., and Schatzbarg, A. F. 1997 Cortisol feedback effects on plasma corticotropin levels in healthy subjects. *Psychoneuroendocrinology* 22 (3) 169-176.
- Posener, J. A., Schildkraut, J. J., Williams, G. H., and Schatzbarg, A. F. 1998 Late feedback effects of hypothalamic-pituitary-adrenal axis hormone in healthy subjects. it Psychoneuroendocrinology 23 (4) 371–383.
- Weitzman, E. D., Fukushima, D., Nogeire, C., Roffwarg, H., Gallagher, T. F., and Hellman, L. 1971 Twenty-four hour pattern of the episodic secretion of cortisol in normal subjects. J. Clin. Endocr. 33 14-22.
- Won, G.S.., Jap, T. S., Chang, S. C., Ching, K. N., and Chiang, C. N. 1986 Evidence for a delayed, integral, and proportional phase of glucocorticoid feedback on ACTH secretion in normal human volunteers. *Metabolism* 35 (3) 254-259.

Pure Appl. Chem., Vol. 74, No. 6, pp. 881–890, 2002. © 2002 IUPAC

Cascade mechanism in a self-regulatory endocrine system. Modeling pulsatile hormone secretion*

Thongchai Dumrongpokaphan and Yongwimon Lenbury[‡]

Department of Mathematics, Faculty of Science, Mahidol University, Thailand

Abstract: Many endocrine systems have been found to incorporate some form of cascade mechanism into their operation. Such a mechanism involves an amplification system where an initial reaction gives rise to the generation of multiple second reactions, each of which sets off multiple third reactions, and so on. Examples will be presented, with special attention paid to the hypothalamus-pituitary-testicular axis. The production and secretion of luteinizing hormone (LH) is governed by the medial-basal region of the hypothalamus. It is well known that the release of LH is a highly regulated process determined by negative and positive feedback, as well as neural components. The presence of gonadatropin-releasing hormone (GnRH) on specific adenohypophyseal cell membrane receptors results in the release of LH, which is then transported systemically to the Leydig cells of the testes. All the factors governing the release of these hormones, as well as a biochemical description of their actions, have not been completely elucidated, nor is the mechanism behind the pulsatile fashion in which the decapeptide GnRH and LH are released clearly explained. We describe how such a cascade mechanism in a self-regulatory system may be modeled and analyzed by a singular perturbation approach, identifying conditions that give rise to episodic hormone secretion or activity. Insightful and valuable interpretations can be made from such analysis of the cascade system.

INTRODUCTION

In recent years, there has been a great surge of interest in the study of how information is represented and transmitted in biological systems, specifically in the new field of bioinformatics. In nerve cells, information is transmitted through electrical impulses, which are sometimes generated as high-frequency bursts, followed by periods of quiescence. These impulses also cause muscles to contract and endocrine cells to secrete hormones. Quite often, bursting or episodic activities are observed in biological systems, particularly in endocrine cells. Attempts to model and simulate such mechanisms most frequently lead to nonlinear differential equations. This presents us with quite a challenge to develop nonlinear systems theory and analytical techniques to qualitatively and quantitatively unravel the intrinsic mechanisms that generate such behavior in these complex systems.

The study of endrocrinology over the past century has been mainly dependent upon the scientific methodologies available to probe the various endocrine systems. Thus, endocrinology has developed from being largely pursued at the physiological level into a biochemical era, which began in approximately 1955–1960 [1] and extends to the present time. Advances in chemical methodology, such as chromatography, mass spectrometry, nuclear magnetic resonance spectroscopy (NMR), and X-ray crystallography, have and continue to permit the detection and chemical characterization of minute quantities (nanograms or picograms) of new hormones and the characterization of the many receptors.

^{*}Plenary lecture presented at the International Conference on Bioinformatics 2002: North-South Networking, Bangkok, Thailand, 6-8 February 2002. Other presentations are presented in this issue, pp. 881-914.

[‡]Corresponding author

T. DUMRONGPOKAPHAN AND Y. LENBURY

With the invention of scanning electron microscopes and confocal microscopy, which allows realtime imaging of living cells, the science of endocrinology is advancing rapidly. Scientists have been busily active in categorizing and defining the scope of influence and molecular mode of action of different hormones, as well as the mechanisms in their secretion.

Many endocrine systems incorporate some form of cascade mechanism into their operation [1]. A system with a cascade mechanism is an amplification process where an initial reaction results in the generation of multiple second reactions, each of which sets off multiple third reactions, and so on.

In this paper, we first discuss two examples of such cascade systems and explain how modeling and analysis of the system may be carried out based on singular perturbation principles. The method utilizes simple geometric arguments based on the assumption of highly diversified dynamics inherent to the cascade system. Application of the technique is done on the hypothalamus—pituitary—testicular axis involved in the biosynthesis and secretion of testosterone in response to blood levels of luteinizing hormone (LH). Episodic release of LH is triggered by the presence of the gonadotropin-releasing hormone (GnRH), secreted from the hypothalamus in a pulsatile fashion [1,2], which we attempt to explain through modeling and analysis. The analysis will then be extended to encompass higher-dimensional systems, which involve a multitude of components or species.

CASCADE HORMONE SYSTEMS

In the following, we describe two examples of systems with cascade mechanism. One classical biochemical cascade mechanism, at the cellular and molecular level, is generated by the action of a hormone, such as the action of glucagon at the cell membrane to produce an increase in cyclic AMP. Figure 1 shows a schematic description of a mechanism leading from the cell surface hormonal signal to the cellular metabolic response: glucagon and glycogenolysis. The cascade may be visualized in terms of alter-

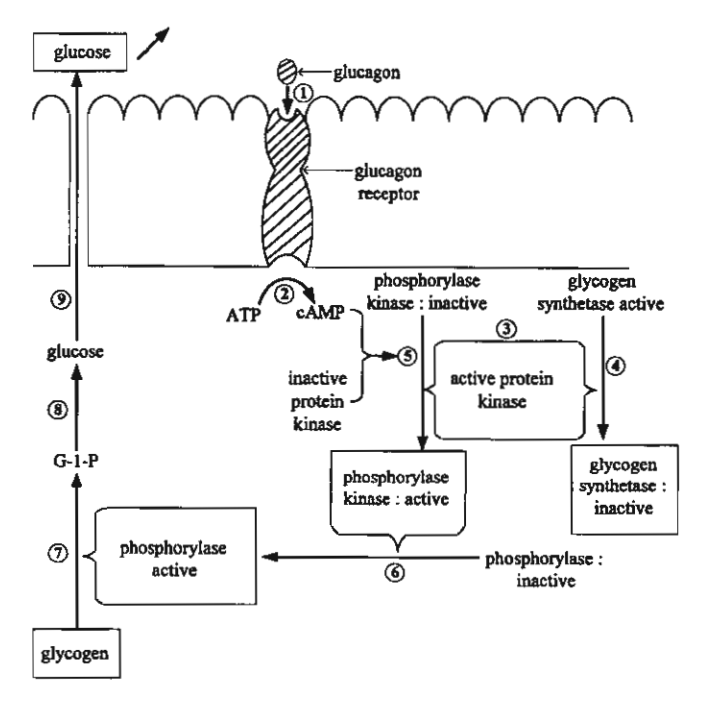


Fig. 1 A schematic description of a mechanism leading from the cell surface hormonal signal to the cellular metabolic response: glucagon and glycogenolysis.

ations of cellular response, stimulation of glycogenolysis to generate glucose for export to the extracellular space, and the general circulating system [1].

As so clearly elucidated by Norman and Litwack [1], the cascade begins with glucagon combining with its cell membrane receptor, marked (1) in Fig. 1. This then stimulates the activity of adenylate cyclase, possibly mediated by a transducing element, on the cytoplasmic side of the membrane, marked (2) in Fig. 1. As a result, the level of cyclic AMP increases, which activates a protein kinase (3), while the protein kinase subunits catalyze the phosphorylation of inactive phosphorylase kinase in reaction (5), as well as the active glycogen synthetase (4), to produce the phosphorylated inactive form, a step marked (6) in Fig. 1. The resulting phosphorylated inactive form consequently stimulates glycogenolysis in step (7) to form glucose 1-phosphate, which is further metabolized to glucose (8). Finally, glucose is transported to the extracellular space and into the general circulation (9). More detailed discussion of each step in the above-described cascade may be found in the work by Norman and Litwack [1]. The system is considered a cascade system due to the fact that each step following hormone binding is mediated by an enzyme that can turn over multiple substrate molecules.

Another system, which also incorporates the cascade mechanism, involves the central nervous system (CNS), the hypothalamus, pituitary, and the distal hormone secretion glands.

As explained by Norman and Litwack in their seminal work on hormones [1], the cascade effect may be produced by a single event or signal in the external or internal environment. A signal can be sent by either electrical or chemical transmission to the limbic system and then to the hypothalamus. This results in the secretion of a releasing hormone into the closed portal system connecting the hypothalamus and anterior pituitary shown in Fig. 2. It has been documented that releasing hormones may be secreted in nanogram amounts and half-lives of about 3–7 min. The releasing hormone consequently

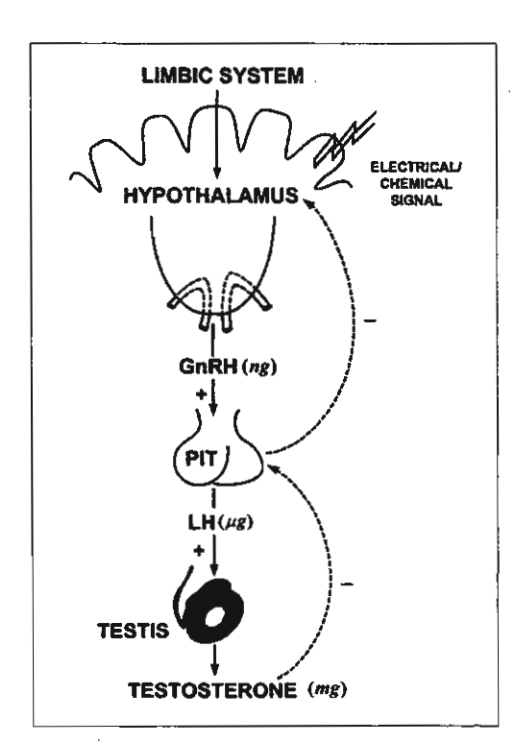


Fig. 2 Diagram showing the cascade hormonal system, the hypothalamus-pituitary-testicular axis, on proceeding down the cascade from the releasing hormone to the terminal hormone, there are increasing masses of the hormones released.

© 2002 IUPAC, Pure and Applied Chemistry 74, 881-890

T. DUMRONGPOKAPHAN AND Y. LENBURY

signals the release of the specific anterior pituitary hormones, which may be secreted in microgram amounts with half-lives on the order of 20 min or longer. The anterior pituitary in turns signals the release of the ultimate hormone, which may be secreted in many micrograms or milligram amounts and can be quite stable.

Thus, amplification of a single event at the outset could prove to be a factor of thousands to a millionfold, as hormone stability and the amounts of hormones increase as we proceed down the cascade.

Three-component cascade system

Letting x(t), y(t), and z(t) represent the densities or levels of the three components at anytime t in the cascade system described above, their rates of production will form a model consisting of the following system of differential equations

$$\dot{x} = f(x, y, z) \tag{1}$$

$$\dot{y} = \varepsilon g(x, y, z) \tag{2}$$

$$\dot{z} = \varepsilon \delta h(x, y, z) \tag{3}$$

where ε and δ are small positive parameters. Thus, when the quantities on the right sides of eqs. 1-3 are finite and different from zero, $|\dot{y}|$ is of the order ε and $|\dot{z}|$ is of the order ε δ . Thus, x is assumed to possess the fastest dynamics, y an intermediate time response, while z possesses the slowest dynamics of the three components.

It is well known that the system (1-3) with small ε and δ can be analyzed with the singular perturbation method [3], which under suitable regularity conditions, allows the approximation of the solution of the system (1-3) with a sequence of simple dynamic transitions occurring at different speeds.

Given an initial condition (x_0, y_0, z_0) , the slow z and intermediate (y) variables are frozen, and the system will develop according to the "fast system".

$$\dot{x}(\tau_1) = f[x(\tau_1), y_0, z_0]$$
 , $\tau_1 = \frac{t}{\varepsilon \delta}$

Thus, $x(\tau_1)$ eventually tends toward a stable equilibrium $\overline{x}(x_0, y_0, z_0)$ of the fast system. Then, as z is still frozen at z_0 , the transitions will develop at intermediate speed according to the "intermediate system"

$$\dot{y}(\tau_2) = g\{\bar{x}[x_0, y(\tau_2), z_0], y(\tau_2), z_0\}$$
, $\tau_2 = \frac{t}{\varepsilon}$

until an equilibrium $\overline{y}(x_0, y_0, z_0)$ of the intermediate system is reached. A third transition then develops at low speed along the curve f = g = 0 to end at an equilibrium or form a closed cycle, depending on the stability properties of the three equilibrium manifolds f = 0, g = 0, and h = 0.

The sequence of these transitions thus constructed then approximates the solution of the system, in the sense that the real trajectory is contained in a tube around the traced transitions, and that the radius of the tube goes to zero with ε and δ . More detail of the main aspects of the method can be found in the work by Muratori and Rinaldi [3], while examples of applications to nonlinear systems in biology and medicine are available in the works of Lenbury et al. [4,5].

Application in modeling pulsatile secretion of LH

The hypothalamus-pituitary-testicular axis is diagrammed schematically in Fig. 2. The release of LH is a highly regulated process determined by (a) negative feedback, (b) positive feedback, and (c) neural components.

Table 1 Relevant information on testosterone.

Biochemical aspects	Data		
Plasma concentration (ng/100 ml)	300–1100		
Testes secretion rate	5000		
Metabolic clearance rate (litre/day)	980		
Site of production	Leydig cells of testes		
Structure	OH OH		
Principal biological function	Maintenance of functional male repro- ductive system and secondary male sex characteristics		

The decapeptide GnRH is released from the hypothalamus in a pulsatile fashion with short latency and initiates the episodic secretion of LH. The LH is then transported systemically to the Leydig cells of the testes. LH-mediated stimulation of testosterone synthesis and secretion by the Leydig cells is initiated by the binding of LH to hormone-specific receptors on the outer membranes of the Leydig cell. The rate of biosynthesis and secretion of testosterone, whose structure is shown in Table 1, is positively correlated with the blood levels of LH, while the secretion of the gonadotropin can be diminished by increasing blood concentrations of testosterone, which facilitates their binding to steroid receptors in both the hypothalamus and pituitary. This is called "suppressive negative feedback". The precise details of the feedback mechanism in this self-regulatory system are not yet clear. Nevertheless, close study of the process has led Liu and Deng [6] to propose a model consisting of the following equations.

$$\frac{dR}{dt} = \frac{a_1 + a_2 R + a_3 R^2}{1 + \alpha_4 T + \alpha_5 T^2 + a_6 R + a_7 R^2} - a_8 R \tag{4}$$

$$\frac{dL}{dt} = \frac{a_9 + a_{10}R}{1 + a_{11}T + a_{12}R} - \alpha_{13}L \tag{5}$$

$$\frac{dT}{dt} = a_{14} + \alpha_{15}L + \frac{\alpha_{16}L + \alpha_{17}L^2}{1 + \alpha_{18}L + \alpha_{19}L^2 + \alpha_{20}RT + \alpha_{21}RLT} - \alpha_{22}T$$
(6)

where R, L, and T are concentrations of GnRH, LH (above the basal level), and testosterone, respectively. The first term in eq. 4 accounts for the autoregulatory effect of GnRH and T on GnRH secretion. The second term represents the removal of GnRH proportional to the amount present, and similarly for all the last terms in eqs. 4–6.

The factor $a_{10}R$ in eq. 5 accounts for the stimulating effect of GnRH on the release of LH, while a_9 accounts for the autonomous secretion of LH independent of GnRH. The term $\alpha_{15}L$ in eq. 6 accounts for the stimulating effect of LH on testosterone secretion, while a_{14} is the secretion rate of T independent of LH. The factors in the denominators of the positive terms in the 3 equations account for autoregulation on the rates of secretion of all 3 hormones.

Taking into account the cascade effect of the system described earlier, we can assume that the time responses of the three components in the above system are quite diversified, and scale the dynamics of the cascade by means of two small dimensionless positive parameters ε and δ as follows. Letting

T. DUMRONGPOKAPHAN AND Y. LENBURY

$$x = R, y = \varepsilon L, z = \varepsilon \delta T, \ a_4 = \frac{\alpha_4}{\varepsilon \delta}, \ a_5 = \frac{\alpha_5}{\varepsilon^2 \delta^2}, \ a_{11} = \frac{\alpha_{11}}{\varepsilon \delta}, \ a_{13} = \frac{\alpha_{13}}{\varepsilon}, \ a_{15} = \frac{\alpha_{15}}{\varepsilon}, \ a_{16} = \frac{\alpha_{16}}{\varepsilon}, \ a_{17} = \frac{\alpha_{17}}{\varepsilon^2}, \ a_{18} = \frac{\alpha_{18}}{\varepsilon}, \ a_{19} = \frac{\alpha_{19}}{\varepsilon^2}, \ a_{20} = \frac{\alpha_{20}}{\varepsilon \delta}, \ a_{21} = \frac{\alpha_{21}}{\varepsilon^2 \delta}, \ \text{and} \ a_{22} = \frac{\alpha_{22}}{\varepsilon \delta}, \ \text{we are led to the following system.}$$

$$\frac{dx}{dt} = \frac{a_1 + a_2 x + a_3 x^2}{1 + a_4 z + a_5 z^2 + a_6 x + a_7 x^2} - a_8 x \equiv f(x, y, z)$$
 (7)

$$\frac{dy}{dt} = \varepsilon \left[\frac{a_9 + a_{10}x}{1 + a_{11}z + a_{12}x} - a_{13}y \right] \equiv \varepsilon g(x, y, z)$$
(8)

$$\frac{dz}{dt} = \varepsilon \delta \left[a_{14} + a_{15}y + \frac{a_{16}y + a_{17}y^2}{1 + a_{18}y + a_{19}y^2 + a_{20}xz + a_{21}xyz} - a_{22}z \right] = \varepsilon \delta h(x, y, z)$$
(9)

We are able to show that the relative positions of the 3 equilibrium manifolds f = 0, g = 0 and h = 0 will be as depicted in Fig. 3 if the following conditions hold:

$$a_8 < a_2 \tag{10}$$

$$a_6 a_8 - a_3 < 0 ag{11}$$

$$a_{15}a_{18}^2 + a_{17}a_{18} + 2a_{15}a_{19} > a_{16}a_{19}$$
 (12)

$$27q^2 + 4p^3 < 0 ag{13}$$

$$4u^3 + 27v^2 > 0 ag{14}$$

$$y_1 < y_m \text{ and } y_M < y_2 \tag{15}$$

where

$$p = \frac{s^2}{3} \tag{16}$$

$$q = t + \frac{2s^3}{27} \tag{17}$$

$$s = \frac{a_6 a_8 - a_3}{2 a_7 a_8} \tag{18}$$

$$t = \frac{a_1}{2a_7 a_8} \tag{19}$$

$$u = c_2 - \frac{c_1^2}{3} \tag{20}$$

$$v = c_3 - \frac{c_1 c_2}{3} + \frac{2c_1^3}{27} \tag{21}$$

$$c_1 = \frac{a_6 a_8 - a_3}{a_7 a_8} \tag{22}$$

887

Cascade mechanism in a self-regulatory endocrine system

$$c_2 = \frac{a_8 - a_2}{a_7 a_8} \tag{23}$$

$$c_3 = -\frac{a_1}{a_7 a_8} \tag{24}$$

while y_1 , y_2 are the y-coordinates of the minimum and maximum points, respectively, on the f = g = 0 curve, and y_m , y_M are those of the f = h = 0 curve, as seen in Fig. 3. Specifically, inequality (15) is the separation condition which ensures that the slow manifold h = 0 separates the two stable branches of the curve f = g = 0 for y in a certain interval containing the point where f = g = h = 0.

The system, initially at a generic point, say point A of Fig. 3, will make a fast O(1) transition, indicated by three arrows, to the stable portion of the slow manifold f = 0 (point B in Fig. 3). As point B is approached, y has slowly become active. An O(ε) transition at intermediate speed, indicated by two arrows, is made along f = 0 in the direction of decreasing y, since g > 0 here, to point C on the stable part of the curve f = g = 0. From point C, a slow O($\varepsilon\delta$) transition, indicated by a single arrow, is then made along this curve in the direction of increasing z, since h > 0 here below the surface h = 0.

Once point D is reached, the stability of the manifold is lost. The O(1) time-scale becomes dominant once again. Hence, the orbit follows a path close to the curve y = constant, z = constant, at high speed, bringing the system to point E on the other stable branch of the manifold f = 0. This is followed by a motion at intermediate speed on f = 0 to point F on the curve f = g = 0 Consequently, the system will slowly develop along this line in the direction of decreasing z, since h is now negative.

At point G on this curve, the stability will again be lost and a fast transition will bring the system back to point H on the stable portion of f = 0, followed by a motion at intermediate speed to point I on the curve f = g = 0, before repeating the same previously described path, thereby forming a closed cycle IDEFGHI. Thus, the existence of a limit cycle in the system for ε and δ sufficiently small is assured. The exact solution trajectory of the system will be contained in a tube about this closed curve, the radius of which tends to zero with ε and δ .

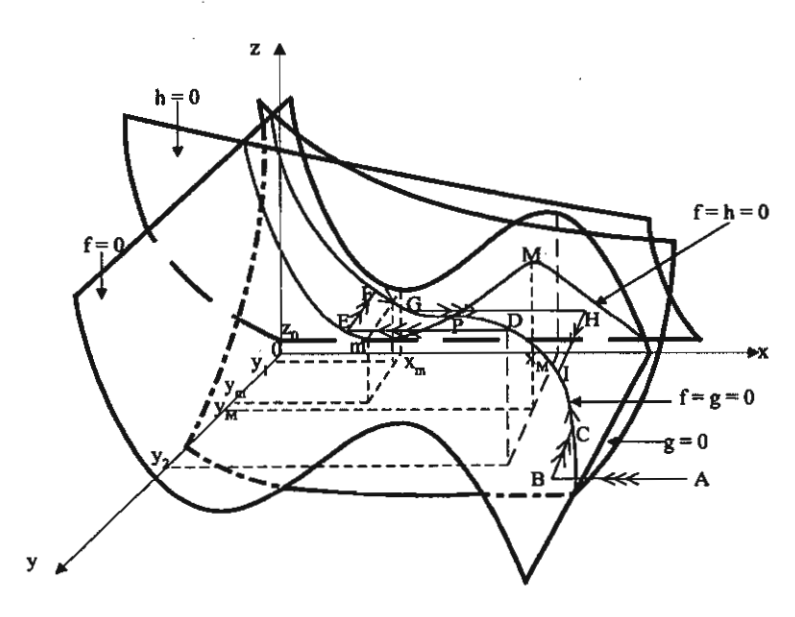


Fig. 3 Shapes and relative positions of the equilibrium manifolds in the case where a limit cycle exists. Here, three arrows indicate fast transitions, two arrows indicate transitions at intermediate speed, and a single arrow indicates slow transitions.

© 2002 IUPAC, Pure and Applied Chemistry 74, 881-890

T. DUMRONGPOKAPHAN AND Y. LENBURY

A computer simulation of eqs. 7-9 is presented in Fig. 4 with parametric values chosen to satisfy the inequalities (10-15). The solution trajectory, projected onto the (y, x)-plane, is seen in Fig. 4a to tend to a limit cycle as theoretically predicted. The corresponding periodic time series of LH is shown in Fig. 4b.

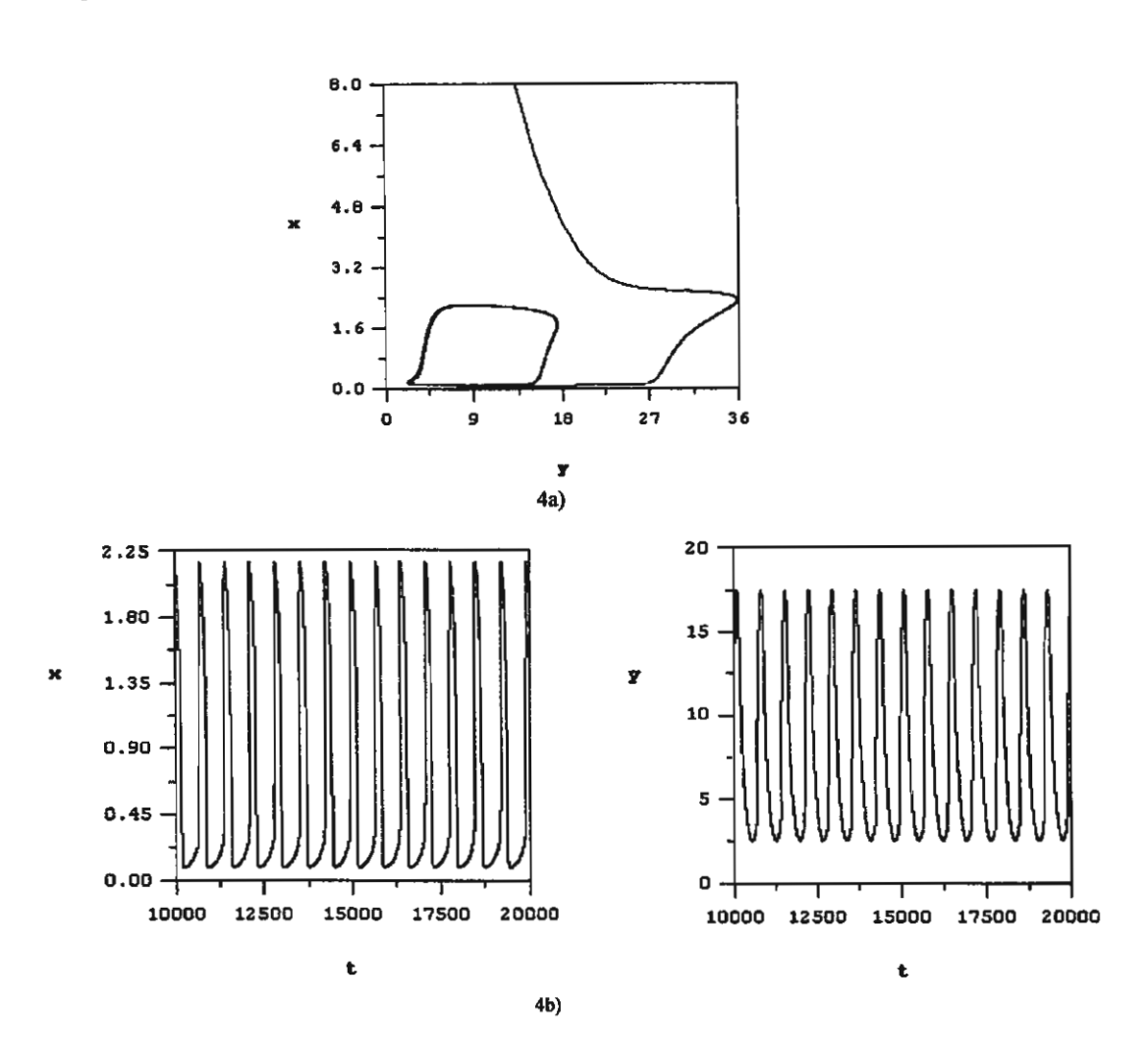


Fig. 4 A computer simulation of the model system of eqs. 7–9 with parametric values chosen to satisfy the conditions identified in the text for which periodic solutions exist. The solution trajectory, projected onto the (y,x)-plane, is seen in (a) to tend toward a stable limit cycle as theoretically predicted. The corresponding time series of GnRH (x) and LH (y) are shown in (b). Here, $\varepsilon = 0.8$, $\delta = 0.05$, $a_1 = 0.2$, $a_2 = 0.1$, $a_3 = 3$, $a_4 = 0.1$, $a_5 = 0.01$, $a_6 = 0.5$, $a_7 = 2$, $a_8 = 0.5$, $a_9 = 0.05$. $a_{10} = 1.5$, $a_{11} = 1.0$, $a_{12} = 0.2$, $a_{13} = 0.01$, $a_{14} = 0.2$, $a_{15} = 0.1$, $a_{16} = 0.1$, $a_{17} = 0.1$, $a_{18} = 0.2$, $a_{19} = 0.2$, $a_{20} = 0.1$, $a_{21} = 0.1$, and $a_{22} = 0.1$.

Extension to higher-dimensional systems

In order to extend the above concept to higher dimensional systems, let us consider a system of n + 3 differential equations which may be written in the form

© 2002 IUPAC, Pure and Applied Chemistry 74, 881-890

Cascade mechanism in a self-regulatory endocrine system 889

$$\dot{x} = F(x, y, z, w; \alpha) \tag{25}$$

$$y = \varepsilon G(x, y, z, w; \alpha)$$
 (26)

$$\dot{y} = \varepsilon \delta H(x, y, z, w; \alpha) \tag{27}$$

$$\dot{w} = \varepsilon \delta \eta \, K(x, y, z, w; \alpha) \tag{28}$$

where ε , δ , and η are small positive constants, $\alpha \in \Re^N$ is the N-dimensional vector of system parameters,

while
$$\begin{bmatrix} x \\ y \\ z \end{bmatrix} \in \Re^3$$
 and

$$w = \begin{bmatrix} w_1 \\ w_2 \\ \vdots \\ w_n \end{bmatrix} \in \Re^N$$

are the n + 3 state variables, and

$$K = \begin{bmatrix} K_{I}(x, y, z, w; \alpha) \\ K_{2}(x, y, z, w; \alpha) \\ \vdots \\ K_{n}(x, y, z, w; \alpha) \end{bmatrix}$$

Hence, x is the fast variable, y the intermediate, z the slow, and w_i , i = 1, 2, ..., n, the very slow components of the system.

Employing the same line of arguments as above, we first assume that w is varying extremely slowly in comparison to the first three components x, y, and z. Then, we may initially assume that w is kept frozen at a constant value w(0) while x, y, and z vary according to the three-dimensional system

$$\dot{x} = F[x, y, z, w(0); \alpha] = f(x, y, z) \tag{29}$$

$$\dot{\mathbf{y}} = \varepsilon G[\mathbf{x}, \mathbf{y}, \mathbf{z}, \mathbf{w}(0); \alpha] = \varepsilon g(\mathbf{x}, \mathbf{y}, \mathbf{z}) \tag{30}$$

$$\dot{y} = \varepsilon \delta H[x, y, z, w(0); \alpha] = \varepsilon \delta h(x, y, z) \tag{31}$$

Thus, if, for suitable parametric values α , the relative positions of the three equilibrium manifolds of the system (29–31) are the same as those three shown in Fig. 3, then trajectories will develop as described earlier. However, as w varies with time, though very slowly, the shapes and positions of the three manifolds shift slowly as time passes. The coordinates of the points m, M, and O are, in this case, $[x_{\rm m}(w;\alpha),y_{\rm m}(w;\alpha),z_{\rm m}(w;\alpha),y_{\rm m}(w;\alpha),y_{\rm m}(w;\alpha),z_{\rm m}(w;\alpha)]$, and $[x_{\rm o}(w;\alpha),y_{\rm o}(w;\alpha),z_{\rm o}(w;\alpha)]$ respectively, since F, G, and G are all functions of G.

Moreover, if we further assume that each of the equations

$$K_i(x, y, z, w; \alpha) = 0, \quad i = 1, 2, ..., n,$$
 (32)

can be solved for z as an explicit function of the other components:

$$z = Z_i(x, y, w; \alpha), \quad i = 1, 2, ..., n,$$
 (33)

T. DUMRONGPOKAPHAN AND Y. LENBURY

then separation conditions are needed to ensure that the manifold H = 0, as well as those described by the equations in (33) are positioned in between the two stable branches of the curve F = G = 0, in order that a limit cycle exists. These conditions are stated in the following theorem, under all the assumptions mentioned above.

Theorem: Suppose that the functions $F(x, y, z, w; \alpha)$, $G(x, y, z, w; \alpha)$, $H(x, y, z, w; \alpha)$, and $K(x, y, z, w; \alpha)$, are continuous, and that the functions $x_{\mathbf{M}}(w; \alpha), z_{\mathbf{M}}(w; \alpha), x_{\mathbf{m}}(w; \alpha), z_{\mathbf{m}}(w; \alpha), x_{\mathbf{O}}(w; \alpha), z_{\mathbf{O}}(w; \alpha)$, and Z_i , i = 1, 2, ..., n, are continuous and bounded. If, for some permissible value of α , and each fixed value of w, there exists a unique equilibrium point O, where F = G = H = 0, and K = 0, such that

$$\sup_{w} x_{\mathrm{m}}(w;\alpha) < \inf_{w} x_{\mathrm{O}}(w;\alpha) \tag{34}$$

$$\sup x_O(w;\alpha) < \inf_w x_M(w;\alpha) \tag{35}$$

$$\sup_{i} z_{\mathrm{m}}(w;\alpha) < \min_{i} \inf_{\Lambda} Z_{i} \tag{36}$$

$$\max_{i} \sup_{\Delta_{i}} Z_{i} < \inf_{w} Z_{M}(w; \alpha)$$
(37)

where the supremum and infemum of Z_i are taken over its domain Δ_i which is a subset of \Re^{n+2} , then a limit cycle exists for the system of eqs. 25-28, provided that ε , δ , and η , are sufficiently small.

CONCLUSION

Analysis of a self-regulatory endocrine system that incorporates a cascade mechanism has been elucidated through modeling and arguments based on the singular perturbation principles that have exploited the highly diversified dynamics of the cascade system. The method decomposes the system into fast, intermediate, and slow components. The slow-motion trajectories lie on the equilibrium manifold of the fast component. The existence of limit cycles characterized by fast transitions between stable equilibria gives rise to periodic solutions. Thus, the temporal secretion patterns often observed in clinical data [1,2] appear to be the effect of the inherent cascade mechanism combined with the mixture of negative and positive feedback autoregulation process, giving rise to a natural frequency in the pulsatile mode of secretion. When this is interfered with by signals from the neural components or other external factors, irregular secretion patterns may result which have been frequently observed clinically [1,2].

The above analysis provides an example of how episodic activities in a cascade system may be modeled and explained. The technique has then been extended to higher-dimensional systems in order to be capable of coping with multiple-component cascades.

ACKNOWLEDGMENT

Appreciation is extended to the Thailand Research Fund for the financial support that made this research project possible (contract number RTA/02/2542 and PHD/0029/254).

REFERENCES

- 1. L. L. Ewing and B. Zirkin. Recent Prog. Hormone Res. 39, 599-632 (1983).
- 2. R. V. Gallo. Biol. Reprod. 24, 771-777 (1981).
- 3. S. Muratori and S. Rinaldi. Siam. J. Appl. Math. 52, 1688-1706 (1992).
- 4. Y. Lenbury, K. Kamnungkit, B. Novaprateep. IMA J. Math. Applied Med. Biol. 13, 1-21(1996).
- 5. Y. Lenbury, R. Ouncharoen, N. Tumrasvin. IMA J. Math. Applied Med. Biol. 17, 243-261(2000).
- 6. B.-Z. Liu and G.-M. Deng. J. Theor. Biol. 150, 51-58 (1991).

Mathematical Medicine and Biology (2005) 22, 99-112 doi:10.1093/imammb/dqh023

Mathematical models for pressure controlled ventilation of oleic acid-injured pigs

P. S. CROOKET

Biomathematics Study Group, Department of Mathematics, Vanderbilt University, Nashville, TN 37240, USA

K. KONGKUL AND Y. LENBURY

Department of Mathematics, Mahidol University, Bangkok, Thailand

AND

A. B. ADAMS, C. S. CARTER, J. J. MARINI AND J. R. HOTCHKISS

Pulmonary and Critical Care Medicine, Regions Hospital and University of Minnesota,

St. Paul, MN 55101, USA

[Received on 31 January 2003; accepted on 1 December 2003]

One-compartment, mathematical models for pressure controlled ventilation, incorporating volume dependent compliances, linear and nonlinear resistances, are constructed and compared with data obtained from healthy and (oleic acid) lung-injured pigs. Experimental data are used to find parameters in the mathematical models and were collected in two forms. Firstly, the P_e -V curves for healthy and lung injured pigs were constructed; these data are used to compute compliance functions for each animal. Secondly, dynamic data from pressure controlled ventilation for a variety of applied pressures are used to estimate resistance parameters in the models. The models were then compared against the collected dynamic data. The best mathematical models are ones with compliance functions of the form C(V) = a + bV where a and b are constants obtained from the P_e -V curves and the resistive pressures during inspiration change from a linear relation $P_r = RQ$ to a nonlinear relation $P_r = RQ^\epsilon$ where Q is the flow into the one-compartment lung and ϵ is a positive number. The form of the resistance terms in the mathematical models indicate the possible presence of gas-liquid foams in the experimental data.

Keywords: oleic acid injury; mathematical model; variable compliance.

1. Introduction

Oleic acid-injured animal models are used to test a wide variety of physiologic approaches and adjunctive therapies in mechanical ventilation (Bowton & Kong, 1989; Hernandez et al., 1990; Wilson et al., 2001). Using animal models of lung injury and disease, researchers have probed acute physiologic and therapeutic techniques ranging from liquid ventilation (Sawada et al., 2002), splanchnic perfusion and oxygenation (Jedlinska et al., 2001), ventilatory support (Martynowicz et al., 2001; Mutch et al., 2000; Nam et al., 2000; Neumann et al., 2000; Neumann & Hedenstierna, 2001) to tracheal gas insufflation or TGI (Carter et al., 2002; Cereda et al., 1999; Zhan et al., 2001). One of the more important uses of oleic acid-injury models is to evaluate the efficacy of recruitment manoeuvres (Cakar et al., 2000; Crott et al., 2001; Martynowicz et al., 2001; Pelosi et al., 2001; Van der Kloot et al., 2000). In this paper we report on

Corresponding Author. Email: philip.s.crooke@vanderbilt.edu

data collected from pigs that were subjected to mechanical ventilation before and after oleic acid injury. Using these data, robust mathematical models of prevailing lung mechanics are constructed that capture the differences in pre- and post-injury physiology of the animals. Such accurate mathematical models allow prediction of key outcome variables of mechanical ventilation: tidal volume, average volume, end-expiratory pressure, mean alveolar pressure, and ventilator power. The physiologic parameters of the animals, compliance and resistance (both inspiratory and expiratory), must be identified so that these quantities can be used in the dynamic mathematical models. Using the static elastic pressure-volume (P_e-V) curves, compliance functions are constructed for each animal and the dynamic data are used to estimate inspiratory and expiratory resistance constants.

The experimental protocol was approved by the Animal Care and Use Committee of Region Hospital; all animals were managed according to NIH standards. In these animal studies, pigs were anesthetized with pentobarbital, paralyzed, and tracheally intubated. Mechanical ventilation was initiated using pressure controlled ventilation with applied pressure (P_{set}) of 10 cm H₂O during inspiration, positive end-expiratory pressure (PEEP) of 5 cm H₂O, FIO₂ of 0·6, and duty cycles of either 1/3, 1/2, or 2/3. Continuous IV general anesthesia and paralysis (pentobarbital and pancuronium) was provided. P_e-V curves were then collected for each animal. The pigs were ventilated using different combinations of duty cycles and applied airway pressures during inspiration (P_{set}) and expiration (P_{peep}); the time, airway pressure, and flow were measured over several cycles of the ventilator. Lung injury was then induced by oleic infusion using a standard protocol and static P_e-V curves again measured. Using the same ventilator settings that were employed before injury, data were again collected for time, airway pressure, and flow.

The mathematical models used to analyse the experimental data are based on a unicompartmental model that permits the compliance of the respiratory system to vary with lung volume: i.e. elastic pressure, P_e , is given by $P_e = F(V)$ where V is the lung volume at any instant of time above its rest volume and F is a function that can be calculated from the P_e-V curves during inspiration and expiration. Furthermore, the models permit the resistive pressure P_r to depend on the flow $Q = |\dot{V}|$ in a nonlinear fashion.

The paper is structured as follows. A brief overview of variable compliance is presented in Section 2, showing that the compliance of the respiratory system can be approximated by continuous linear functions of the volume V. In Section 3, a mathematical model for pressure controlled ventilation with variable compliance, linear and nonlinear resistances is then constructed. In the clinical setting, the clinician sets the levels of applied airway pressures (P_{set} and P_{peep}), frequency of breathing (f), and the inspiratory time fraction or duty cycle (D) while the compliance (C) and resistances (R_i and R_e) are uncontrolled variables. The key outcome variables of the ventilation are the tidal volume (V_T), minute ventilation (\dot{V}_E), end-expiratory pressure (P_{ex}), mean alveolar pressure (P_m), and power (\dot{W}_m). These quantities are computable from the mathematical model.

Data for the validation of the mathematical models were sampled from data collected in other studies at Region Hospital. Although the database included several animals, in this paper we restrict our discussions to three pigs (labelled A, B, C). The ideas presented here were tested on other animals and found to be consistent with the data sets from the three pigs. For brevity, we do not include the extra data.

TABLE 1 One-segment compliance function parameters for inspiration and expiration, pre- and post-injury, for a particular animal (Pig A)

	Pre-injury		Post-	injury
Parameter	Inspiration	Expiration	Inspiration	Expiration
aj	0.0419	0.0952	0.0121	0.103
b_j	-0.00272	-0.0388	0.0241	-0.0449

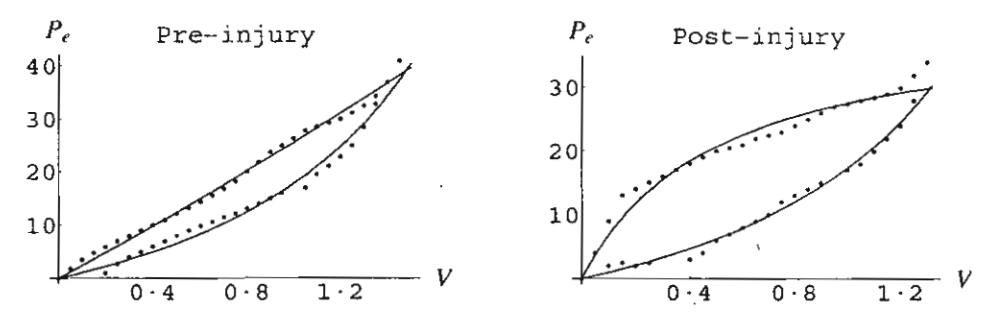


Fig. 1. P_e -V data for a particular animal (Pig A) approximated by a one-segment compliance function.

2. A variable compliance model for the P_e-V curves

In Crooke et al. (2002), a variable compliance model was proposed for pressure controlled ventilation. In its simplest form, it assumes that the elastic pressure in the lungs is of the form

$$P_e = \frac{V}{a+bV} \tag{2.1}$$

where P_e denotes the elastic pressure in the one-compartment lung, V is the volume of the compartment above its rest volume, and the parameters, a and b, are obtained from experimental data. In the collection of the elastic pressure-volume data, it is assumed that the end-expiratory pressure of the lung is zero. In other words, these data were collected without applied PEEP after a protracted exhalation minimizing auto-PEEP.

We call the linear function, C(V) = a + bV, the compliance function of the model. Since, in fact, $C = \frac{dV}{dP}$, the approximation C(V) = a + bV is only accurate provided $\frac{bV}{a} \ll 1$. If C varies too quickly with V, the physical data for the compliance function may deviate significantly from the linear approximation a + bV. The parameters, a and b, of the compliance function during inspiration may be different from those during expiration. That is, there is hysteresis. During passive ventilation, C represents the compliance of the total respiratory system, lungs and chest cavity. Because during these experiments, the animals were pharmacologically paralyzed, this is an appropriate assumption. In Fig. 1, each $P_e - V$ curve (inspiration/expiration and pre/post-injury) for a particular animal (Pig A) is approximated by functions of the form $P_e = V/(a + bV)$ with a and b chosen to give the best least squares fit. The constants for this data set are listed in Table 1. As can be seen in Fig. 1, we obtain a reasonable fit of the experimental data, although there is some error at the extremes of the curves. However, as will be seen in later sections, our model is found to uniformly produce good approximations to experimental data.

3. Models for pressure controlled ventilation

Along with the P_e-V data collected for each animal in this study, pressure controlled ventilation data was collected for a variety of P_{set} and P_{peep} combinations using breaths of 6 s in length and an inspiratory time fraction or duty cycle of either 1/3, 1/2, or 2/3. In this section we attempt to match the data with a variety of mathematical models for controlled preset ventilation.

Several mathematical models for pressure controlled ventilation of a single compartment lung were examined. It is assumed that breaths are identical and are of duration t_{tot} . Each breath is subdivided into an inspiratory phase of length t_i and expiratory phase of length t_e so that $t_{tot} = t_i + t_e$. At any instant of time in $[0, t_{tot}]$, there is a pressure balance between applied pressures or ventilatory pressures (P_{vent}) , pressures due to elastic forces (P_e) , pressures due to resistive losses (P_r) , and the end-expiratory pressure (P_{ex}) :

$$P_r + P_e + P_{ex} = P_{vent}$$

In this model, the symbol V(t) represents the volume above the volume of the lung at the end of the previous breath. Hence, V(t) is referenced to a constant volume V_{ex} which is explained below. Assuming breaths of uniform length (t_{tot}) , V(t) is zero at the beginning and ending of each breath. We define the end-expiratory volume (V_{ex}) to be the volume of the lung above its rest volume due to P_{ex} ; that is, $P_{ex} = V_{ex}/C(V_{ex})$. We denote by $V_i(t)$ the volume of the compartment above V_{ex} during inspiration and by $V_e(t)$ the compartmental volume above V_{ex} during expiration. We assume that $V_i(0) = V_e(t_{tot}) = 0$. V_T denotes the tidal volume and it is assumed that $V_T = V_i(t_i) = V_e(t_i)$. For the elastic pressure, we assume that $P_e = V/C(V)$ where C(V) is the compliance function discussed in the previous section. For the resistive pressure, we assume that $P_r = RQ^e$ where Q is the flow into or out of the lung, i.e. Q = |dV/dt|, R is a constant, and e is a positive parameter. We allow R, e, and e obtains applied to the airway, e of the next breath, e of the next breath and of the next breath of the next breath, e of the next breath and the next breath of the

Inspiration:

$$R_i \left(\frac{\mathrm{d}V_i}{\mathrm{d}t}\right)^{\epsilon_i} + \frac{V_i}{C_i(V_i)} + P_{ex} = P_{set}, \ 0 \leqslant t \leqslant t_i$$
 (3.1)

Expiration:

$$-R_e \left(\left| \frac{\mathrm{d}V_e}{\mathrm{d}t} \right| \right)^{\epsilon_e} + \frac{V_e}{C_e(V_e)} + P_{ex} = P_{peep}, \ t_i < t \leqslant t_{tot}. \tag{3.2}$$

Differential equation (3.1) has the initial condition $V_i(0) = 0$ and (3.2) requires $V_e(t_i) = V_T$. The constant P_{ex} (end-expiratory pressure) is determined by the boundary condition $V_e(t_{tot}) = 0$. The relationship between P_{ex} and V_{ex} is given by $P_{ex} = V_{ex}/C_e(V_{ex})$.

Special cases of the above model have been treated in the literature. In the case when $\epsilon_i = \epsilon_e = 1$ and $C_i(V) = C_e(V) \equiv C$, analytical solutions of the system of differential equations can be found (see e.g. Burke *et al.*, 1993; Marini & Crooke, 1993); for $\epsilon_i = \epsilon_e = 1/2$ or 2 and $C_i(V) = C_e(V) \equiv C$, see Crooke & Marini (1993); and when $\epsilon_i = \epsilon_e = 1$ and $C_i(V)$ are piecewise linear functions of V, see Crooke *et al.* (2002).

Data collected for the pre- and post-injury experiments are composed of ventilator delivered and retrieved volume, flow, and airway pressure, sampled every 0.025 s. Various combinations of applied

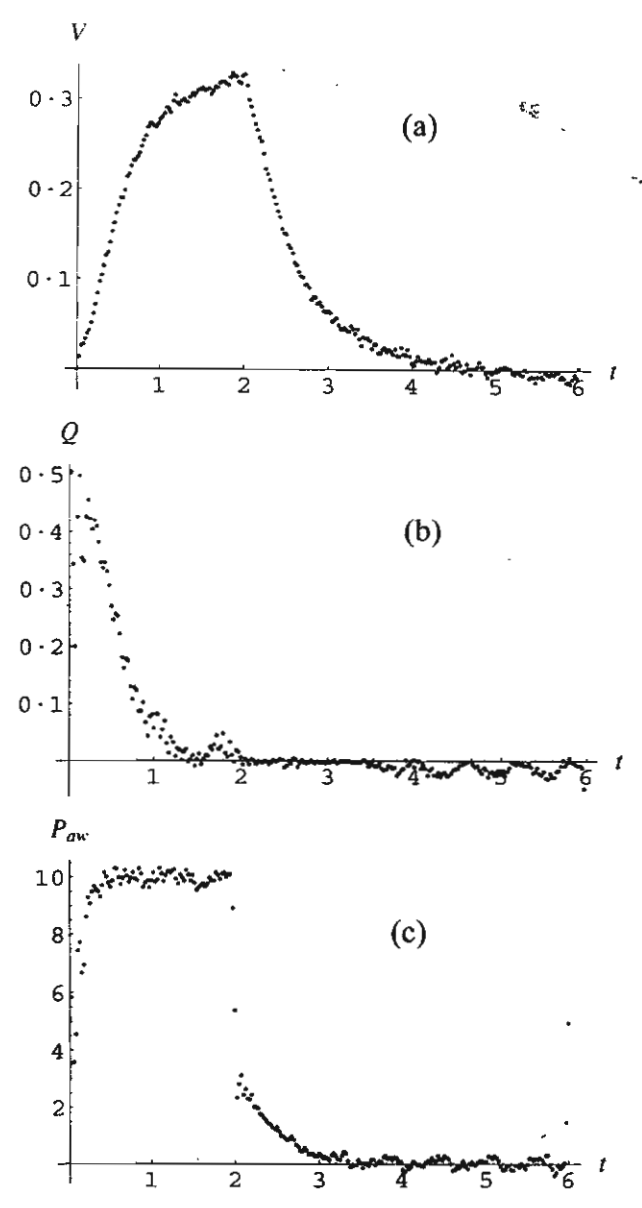


Fig. 2. Experimental data for a pre-injury pig (Pig B) with $P_{set} = 10 \text{ cm H}_2\text{O}$, $P_{peep} = 0 \text{ cm H}_2\text{O}$, $t_{tot} = 6 \text{ s}$, D = 1/3. The collected data for volume, flow, and airway pressure are presented in (a), (b), and (c), respectively.

pressures (P_{set} and P_{peep}) and inspiratory time fraction ($D = t_i/t_{tot}$) were used for ventilator settings. A sample of the collected data (volume, flow, and airway pressure) is pictured in Fig. 2.

If we assume that the dynamic behaviour of the physical system is modelled by the differential equations (3.1) and (3.2), then the unknown resistances, R_i and R_e , in theory, can be obtained from the

experimental data. For example, if we assume that the resistive pressure, P_r , is directly proportional to an exponential power of the flow during inspiration or expiration, then

$$P_r^{(i)} = R_i Q_i^{\epsilon_i} = P_{set} - P_{ex} - \frac{V_i}{C_i(V_i)}$$
 (3.3)

$$P_r^{(e)} = R_e Q_e^{\epsilon_r} = -P_{peep} + P_{ex} + \frac{V_e}{C_e(V_e)}$$
 (3.4)

where V_i , V_e , Q_i and Q_e are lung volumes and the flows in and out of the lung during inspiration and expiration, respectively. In (3.3) and (3.4), we assume that $P_{ex} \approx P_{peep}$ and the compliance functions are obtained from the P_e -V data. The resistive pressure can then be plotted *versus* the flow and volume and a nonlinear regression algorithm used to estimate R_i , R_e , ϵ_i , and ϵ_e . Significant variability in the data can occur for a particular animal and among the various data sets. This is primarily a problem in the expiratory data since the flow levels are small and subject to experimental error. Furthermore, the resistive pressure dependence on the flow must be checked for different dynamic settings: P_{set} , P_{peep} , and D.

Various models (i.e. different combinations for ϵ_i and ϵ_e) were investigated. The accuracy of (3.2) with $\epsilon_e = 1$ was universally good over the various data sets. The accuracy of (3.1) with $\epsilon_i = 1$ in some cases seem to deteriorate at a particular point in the time during inspiration, which we denote by t_{i_1} . We speculated that a new and different dynamics is in control for $t_{i_1} \leq t \leq t_i$. The difference was assumed to reside solely in the resistive pressure behaviour during inspiration. This led us to a new hybrid model which is defined by the differential equations (3.5)–(3.7). In particular, the model assumes that there is a change in the resistance law during inspiration from $P_r = RQ^{\epsilon_{i_1}}$ to $P_r = RQ^{\epsilon_{i_2}}$. The change-over time, t_{i_1} , was found from the experimental data. The initial conditions for each differential equation are $V_{i_1}(0) = 0$, $V_{i_2}(t_{i_1}) = V_{i_1}(t_{i_1})$, and $V_e(t_i) = V_{i_2}(t_i)$. In particular, we have

Inspiration:

$$R_{i_1} \left(\left| \frac{dV_{i_1}}{dt} \right| \right)^{\epsilon_{i_1}} + \frac{V_{i_1}}{C_i(V_{i_1} + V_{ex})} + P_{ex} = P_{set}, \ 0 \le t \le t_{i_1}$$
 (3.5)

$$R_{i_2} \left(\left| \frac{dV_{i_2}}{dt} \right| \right)^{\epsilon_{i_2}} + \frac{V_{i_2}}{C_i(V_{i_2} + V_{ex})} + P_{ex} = P_{set}, \ t_{i_1} < t \le t_i$$
 (3.6)

Expiration:

$$-R_e \left(\left| \frac{\mathrm{d}V_e}{\mathrm{d}t} \right| \right)^{\epsilon_e} + \frac{V_e}{C_e(V_e + V_{ex})} + P_{ex} = P_{peep}, \ t_i < t \leqslant t_{tot}. \tag{3.7}$$

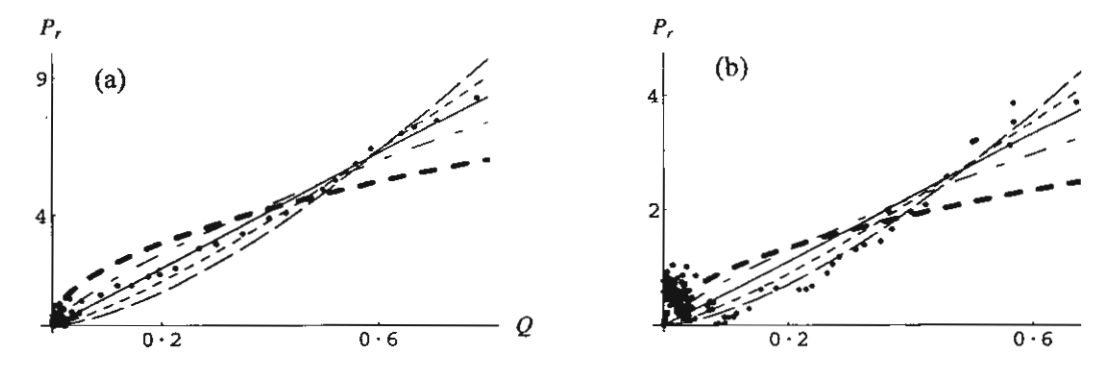
The values of ϵ_{i_1} , ϵ_{i_2} , ϵ_e , together with R_{i_1} , R_{i_2} , and R_e , were found by nonlinear regression of resistive pressure—flow data. The value of the change-over time t_{i_1} was taken also from observed data to be the time at which an abrupt change in the slope of the resistive pressure—flow curve occurs. If this change is not observed in the data, which is the case for most of our pre-injury data, then the change-over time t_{i_1} is set equal to t_i .

In Fig. 3, we present an example of the regression fit of P_r-Q curves of both inspiration and expiration periods for a pre-injury data set, showing curves using five different values of ϵ . For this particular animal (Pig C), we found $t_{i_1} = t_i = 2$ s in the pre-injury data, so that the inspiration period consists of only one part, namely $0 \le t \le t_i$, in which $\epsilon_{i_1} = 1$ and $R_{i_1} = 10.3615$ yielded the least sum

TABLE 2 The values of respiratory resistances, R_i and R_e , obtained for five different values of the flow exponents (ϵ) for inspiratory period and expiratory period of a particular pre-injury pig (Pig B). The Sum of Squares and Mean Square are from the Mathematica ANOVA table used in the nonlinear regression

		Inspiration		
ε_{i_1}	R_{i_1}	Sum of Squares	Mean Square	
0-50	6-68892	45.7886	0-6024820	
0.75	8-70176	10.9364	0.1439000	
1.00	10-3615	4.77519	0-0628315	
1.25	11-9432	7-54956	0.0993364	
1.50	13-5367	13-9685	0.1837960	
		Expiration		
ε_e	Re	Sum of Squares	Mean Square	
0.50	3.00691	34-3241	0.220026	

		Expiration			
ϵ_e	Re	Sum of Squares	Mean Square		
0.50	3.00691	34-3241	0.220026		
0.75	4.33729	26.0255	0.166830		
1.00	5-52216	25.5054	0.163496		
1-25	6.68317	26.9782	0-172937		
1.50	7.90083	28-8444	0.184900		



of squares, compared with the other values of ϵ_{i_1} tried, as can be seen in Table 2. During the expiration period for this pre-injury case (Fig. 3), $\epsilon_e = 1$ and $R_e = 5.52216$ yielded the least sum of squares, as can be seen in Table 2, as well.

In Fig. 4, we present an example of the nonlinear regression fit of P_r-Q curves of inspiration and expiration periods for a post-injury data set, showing curves using five different values of ϵ . Here, we found $t_{i_1} = 0.525$ with $t_i = 4$, so that the inspiration period is split into two parts; one during $0 \le t \le t_{i_1}$ and the other during $t_{i_1} < t \le t_i$. During the first part, we found $\epsilon_{i_1} = 1$ and $R_{i_1} = 17.3134$, while

TABLE 3 The values of respiratory resistances. R_{i_1} , and R_e , obtained for five different values of the flow exponents (ϵ) for the first part of inspiration, $0 \le t \le t_{i_1}$, second part of inspiration, $t_{i_1} < t \le t_i$, and the expiration period, $t_i < t \le t_{tot}$ of a particular post-injury pig (Pig C)

		Inspiration			
		$0 \leqslant t \leqslant t_{i_1} = 0.525$			
ε_{i_1}	R_{i_1}	Sum of Squares	Mean Square		
0.50	16-9763	170-854	8-54272		
0.75	17-4100	41.5195	2.07597		
1.00	17.3134	21.0766	1.05383		
1.25	16.8154	79.8231	3.99116		
1.50	16-0472	189-879 9-4939			
		$0.525 < t \leqslant t_i = 4$			
ϵ_{i_2}	R_{i_2}	Sum of Squares	Mean Square		
0.05	4.20541	516-723	3.717430		
0-25	8.85992	225.081	1-619290		
0.50	18-3022	72-1459	0.519035		
0.75	29.4639	251-702 1-8103			
1.00	37-5697	664-919	4.783590		
		Expira	ition		
		$t_i < t \leqslant t_{tot} = 6$			
ε_e	R_e	Sum of Squares	Mean Square		
0-50	3.17990	22.1118	0-2871660		
0-75	3-54351	6-62740	0.0860701		
1.00	3-66977	5-44785 0-0707			
1.25	3.65902	10.7329	0.1393890		
1.50	3.56458	19-1001	0.2480530		

in the second part, $\epsilon_{i_2} = 0.5$ and $R_{i_2} = 18.3022$ are the best choice, as shown in Table 3. During the expiration period of this post-injury case (Pig C), $\epsilon_e = 1$ and $R_e = 3.6698$ gave the best fit.

We carried out the fitting of $P_r - Q$ curves from several other animals, apart from the ones shown here, and found that using different data sets still yielded the resistive pressure exponent values close to those found for the data set of Pig C shown in Figs. 3 and 4. In other words, the resistive pressure exponent ϵ , in each separate part of the breathing cycle, is not extremely sensitive to variations of different data sets, not changing very much from one animal to another that exhibit similar modes of gas exchange. Thus, it appears that the resistive pressure exponent ϵ is a constant characteristic to a specific flow dynamics and does not mirror the varying of physical data sets, while the nonlinear resistance R is the system parameter which reflects such variations through the process of least squares fitting.

In all our experiments, constant pressure ventilation was used. That is, the applied pressure to the airway is constant during inspiration. In the airway pressure data, the measurement of the applied airway pressure by sensors is for a sudden zero pressure to P_{set} at the beginning of inspiration and then a sudden return in zero pressure at the end of inspiration. Although a slight variation from constant pressure at the beginning and ending of inspiration is usually encountered, this was in fact found to have no significant effect on the resistive pressure exponent ϵ . This is indeed borne out by the observations made by some

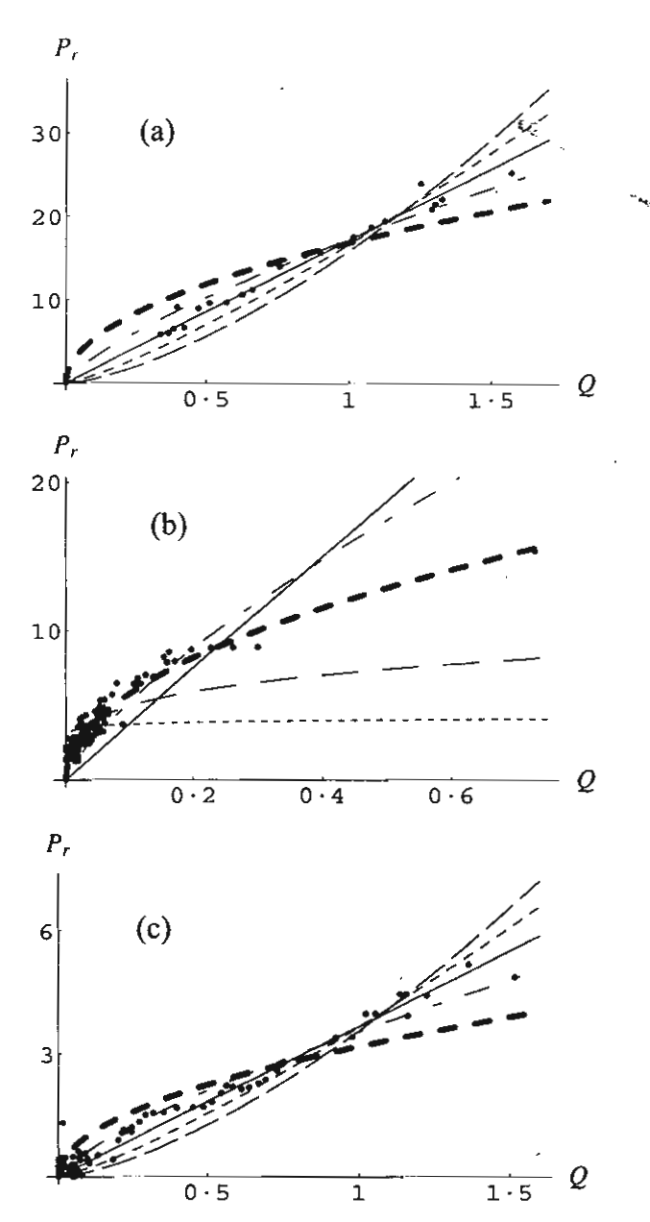


FIG. 4. Curve fitting of resistive pressures during the first part of inspiration (a), second part of inspiration (b) and expiration (c) for post-injury case with different values of parameters $(R_{i_1}, R_{i_2}, R_{\epsilon}, \text{ and } \epsilon)$ given in Table 3. Here, $P_{set} = 25 \text{ cm H}_2\text{O}$, $P_{peep} = 5 \text{ cm H}_2\text{O}$, $t_{tot} = 6 \text{ s}$, and D = 2/3, while $t_{i_1} \neq t_i$. For (a), (b), and (c); $- - \epsilon = 1.5$, $- - \epsilon = 1.25$, $- - \epsilon = 0.75$, $- - - \epsilon = 0.5$, $- - - \epsilon = 0.5$, $- - - \epsilon = 0.5$, and $- \epsilon = 0.5$



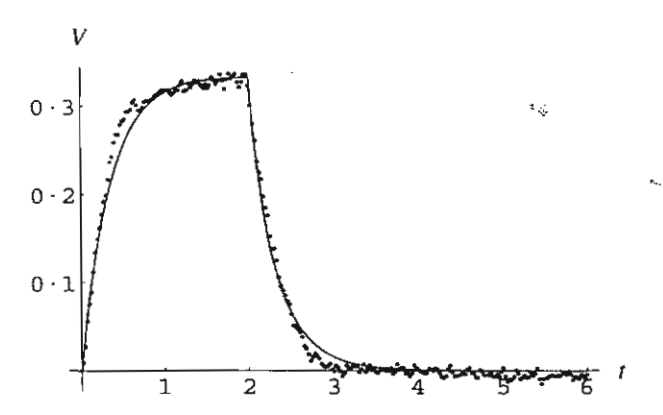


Fig. 5. Comparison of model simulation and experimental data for a particular pre-injury pig (Pig C) of Fig. 3. Here, $t_{i_1} = t_i = 2$ s, $R_{i_1} = 10.3615$ cm H₂O/l/s, $R_e = 5.52216$ cm H₂O/l/s, and $\epsilon_{i_1} = \epsilon_e = 1$ (see Table 2). The solid line corresponds to the model prediction of the lung volume, while the dots are data obtained from the experiment over one breathing cycle.

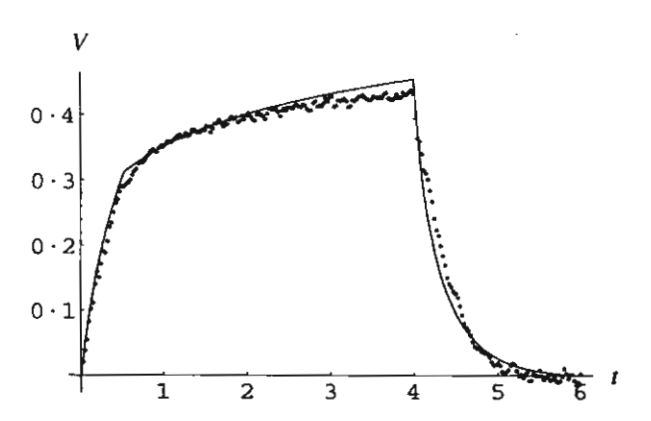


FIG. 6. Comparison of model simulation and experimental data for a particular post-injury pig of Fig. 4 (Pig C). Here, $t_{i_1} = 0.525$ s, $t_i = 4$ s, $R_{i_1} = 17.3134$ cm $H_2O/l/s$, $R_{i_2} = 18.3022$ cm $H_2O/l/s$, $R_e = 3.66977$ cm $H_2O/l/s$, $\epsilon_{i_1} = \epsilon_e = 1$, and $\epsilon_{i_2} = 0.5$ (see Table 3). The solid line corresponds to the model prediction of the lung volume, while the dots are data obtained from the experiment over one breathing cycle.

earlier researchers mentioned by Smith et al. (1991) that there was no convincing physiologic evidence of an advantage on gas exchange derived from a given inspiration gas flow pattern. According to these researchers, there were no significant differences in gas exchange or dynamics between various air flow waveforms. In view of this and our earlier discussion on the sensitivity of the resistive pressure exponent, which appears to be characteristic of a specific flow structure, our assumption of a square wave form, and the slight variation thereof, were found to have little effect on the exponent, as expected.

The model (3.5)–(3.7), with ϵ and R found as described above, was then used to compare with preinjury and post-injury data of volume versus time. These comparisons with the experimental data are shown in Figs. 5 and 6, respectively. The hybrid model was used for other sets of experimental data and uniformly produced accurate approximations. Thus, this defines a class of models that is mathematically tractable and capable of accurate simulations of mechanical ventilation of normal and diseased lungs.

TABLE 4 Theoretical tidal volumes, end-expiratory pressures, mean alveolar pressures, and average lung volumes for different levels of applied PEEP using the hybrid model of Figs. 3 and 4 for both pre-and post-injury cases of a particular animal (Pig C)

Pre-injury			Post-injury					
PEEP	V_T	P_{ex}	P_m	Vave	v_T	P_{ex}	P_m	Vave
0.0	0.66529	0.00473	6-13007	0.55141	0-62441	0.15164	13.22760	0.49562
1.0	0.63207	1.00310	6-82353	0.52392	0.58600	1.10617	13.71900	0.51424
2.0	0.59884	2.00203	7-51701	0-49641	0-54978	2.07399	14.20520	0.44356
3.0	0.56559	3.00132	8-21049	0.46889	0.51569	3.05139	14.68590	0.41915
4-0	0.53233	4.00086	8.90398	0.44136	0.48361	4-03561	15.16080	0.39581
5.0	0.49907	5.00056	9.59747	0.41381	0.45340	5.02464	15.63000	0.37606

Having mathematical expressions for $V_i(t)$ and $V_e(t)$ permits the calculation of tidal volume V_T , average volume V_{ave} , minute ventilation V_E , end-expiratory pressure P_{ex} , and mean alveolar pressure P_m . In particular, $V_T = V_i(t_i)$, P_{ex} is determined from solving $V_e(t_{tot}) = 0$, and the other two outcomes are defined by

$$V_{ave} = \frac{1}{t_i} \int_0^{t_i} V_i(t) \, \mathrm{d}t$$

and

$$P_m = \frac{D}{t_i} \int_0^{t_i} \frac{V_i(t)}{C_i(V_i(t) + V_{ex})} dt + \frac{1 - D}{t_e} \int_{t_i}^{t_{tot}} \frac{V_e(t)}{C_e(V_e(t) + V_{ex})} dt + P_{ex}.$$

In Table 4, theoretical values for these quantities using the hybrid model simulations shown in Figs. 3 and 4, before and after injury, are shown. As one can see, there are substantial reductions in the tidal and average volumes at different PEEP levels. At each level of PEEP, the reductions in tidal and average volumes are approximately 5%. However, approximately 75% of the beginning (PEEP = 0) tidal and average volumes still remains at the last level of PEEP (PEEP = 5 cm H_2O). One possible explanation of the drop-off in volumes from pre- to post-injury is the large resistance, R_{i2} , in the post-injury simulations. Although we do not show the calculation in this paper, it is possible to investigate changes in the key outcome variables as functions of f and D. This could give the clinician insights into the optimal choice of f and D to ventilate at a given P_{set} and P_{peep} .

4. Discussion and conclusion

An interesting speculation about the physiology during this mechanical ventilation (pre- and post-injury) comes from the use of nonlinear resistive pressure $P_r = RQ^{\epsilon}$. It was shown in Deshpande & Barigou (2000) that the flow of gas-liquid foams in vertical pipes follows the rheological relationship

$$\Delta P = k \frac{16LQ_F^n}{\pi \rho^4}$$

where ΔP is the pressure drop along the pipe, ρ is the radius of the circular pipe, L is its length, k is a constant, and Q_F is the steady flow of the foam-liquid. The parameter n is a number in the interval [0.4, 0.9] with its exact value depending on the foam structure, liquid viscosity, and concentration. The hybrid model fits the experimental data quite well in the inspiratory time interval $[t_{i_1}, t_i]$, especially for the post-injury data sets, perhaps because the airways of the lungs of the pigs are filled with gas-liquid

foam due to edema (the lung failure condition caused by the accumulation of the fluid in the lungs). The magnitude of R_{i_2} can then be used to indicate the severity of the edema which is a result of the oleic injury and/or the ventilator induced injury. This hypothesis may have important clinical implication since the model seems to agree well with experimental data (Hubmayr, 2002).

Our curve fitting in the pre-injury case invariably yielded $t_{i_1} = t_i$ and $\epsilon_i = \epsilon_{i_1} = 1$ during the inspiration period, with the exception of only a few cases where t_{i_1} was found to be a little less than t_i . In such a case then $\epsilon_{i_1} = 1$ and $\epsilon_{i_2} = 0.5$, or very close to it. We speculate that, although this is a pre-injury data set, a short period of liquid-foam flow may have resulted from an injury induced by prolonged ventilation with too high an applied pressure, before being subjected to oleic acid injury. As Scarpelli (2003) has asserted in his discussion of the physiology of the alveolar surface network (ASN) that ASN is the totally fluid continuum circulating through ultrathin molecular conduits formed by appositions of unit bubbles of alveolar gas. In fact, ASN is the analogue of foam in vitro, and operates in all regions of the lung, at all lung volumes, beginning at birth and continuing throughout life. The characteristics of alveolar flooding are then explained by the ASN conformation. According to Scarpelli (2003), they are analogous to liquid-overloading of an established foam in vitro to produce 'froth', in which the ratio of continuous phase (liquid) to dispersed phase (gas in unit bubbles) is significantly increased.

In fact, one function of the pulmonary surfactant system is stabilization of the fluid balance in the lung and protection against lung edema. However, it has been shown that mechanical ventilation can damage the lungs when a mode of ventilation that allows high inspiration lung volumes and low levels of positive PEEP is applied (Vazquez de Anda & Lachmann, 2001), leading to loss of surfactant from the airways and eventually pulmonary edema.

The present work presents one-compartment mathematical models of respiratory systems, incorporating variable compliances and nonlinear resistances. The predictions of the hybrid model were compared against experimental data and were found to uniformly produce accurate approximations. Desired outcomes of mechanical ventilation are a minute ventilation \dot{V}_E that is adequate to protect the systemic pH (via removal of CO₂) and a mean alveolar pressure which is sufficient to maintain lung volume and support adequate oxygenation. In Table 4, the tidal volume V_T , end-expiratory pressure P_{ex} , mean alveolar pressure P_{mi} , and average lung volume V_{ave} , are shown for different levels of PEEP, using $P_{set} = 20$ cm H_2O , $t_{tot} = 6$ s, and $t_i = 2$ s in pre-injury case and $P_{set} = 25$ cm H_2O , $t_{tot} = 6$ s, and $t_i = 4$ s in post-injury case. These calculations demonstrate the usefulness of a mathematical model as a means to experiment with the ventilation parameters to achieve the desired levels for the outcome variables. The increase in applied PEEP is observed here to lower the tidal volume and the average lung volume in both the pre-injury and post-injury cases. However, the magnitude of this change varies with the injury.

It is worth nothing that incorporating a variable compliance and the nonlinear resistance was critical to obtain models that accurately portrayed the experimental data. With all the caveats of using a one-compartment model for a complex physical system, the mathematical model may indicate important physiologic processes that are present in injured lungs. For example, is the value of t_{i_1} in the interval $[0, t_i]$ and/or the magnitude of R_{i_2} an indication of the level of injury? Alternatively, are shifts in the parameters, a_j and b_j , of the compliance function indicative of injury and if so, what is the level of injury?

We have developed a hybrid model, depicted in (3.5)–(3.7), which is very robust, mathematically tractable, and capable of accurate simulations of mechanical ventilation of normal and injured lungs. The model will be used to study effects of clinical-set inputs on the key ventilation outcome variables.

An example of why such approaches may be useful is the controversy concerning appropriate treatment of ARDS patients in ARDSNet studies (Stewart, 2002). The National Institute of Health

has recently stopped these trials involving 20 medical institutions because it is difficult to determine if the patients in the control group were receiving inferior treatment. An outcome based analysis of the ARDSNet trails, along with four other independent studies, raised questions about the effectiveness of low tidal volume ventilation on patient mortality (Eichacker et al., 2002). There is great variation from patient to patient and treatment to treatment between studies. Accounting for this variability is difficult and making judgements of the effectiveness of low tidal volume ventilation by this top-down approach to the data is problematical. If it was possible to measure, non-invasively and instantaneously, physiologic parameters whose values indicate the level of lung injury during mechanical ventilation, then some of the uncertainty of the treatment could be resolved. Furthermore, having the resistance and compliance parameters permits calculation of important lung pressure variables such as the peak and mean alveolar pressure, key predictors of lung injury.

Acknowledgements

Kongkul was supported by Ministry of University Affairs, Thailand. Lenbury was supported by The Thailand Research Fund. Marini was supported in part by Health Partners Research Foundation and Hotchkiss is a Scientist Development Grantee of the American Heart Association.

REFERENCES

- BOWTON, D. L. & KONG, D. L. (1989) High tidal volume ventilation produces increased lung water in oleic acid-injured rabbit lungs. Crit. Care Med., 17, 908-911.
- BURKE, W. C., CROOKE, P. S. et al. (1993) Comparison of mathematical and mechanical models of pressurecontrolled ventilation. J. Appl. Physiol., 74, 922-933.
- CAKAR, N., VAN DER KLOOT, T. et al. (2000) Oxygenation response to recruitment maneuver during supine and prone positions in an oleic acid-induced lung injury model. Am. J. Respir. Crit. Care Med., 161, 1949–1956.
- CARTER, C. S., ADAMS, A. B. et al. (2002) Tracheal gas insufflation during late exhalation reduces PaCO₂ in experimental acute lung injury. Inten. Care Med., 28, 504-508.
- CEREDA, M. F., SPARACINO, M. E. et al. (1999) Efficacy of tracheal gas insufflation in spontaneously breathing sheep with lung injury. Am. J. Respir. Crit. Care Med., 159, 845-850.
- CROOKE, P. S. & MARINI, J. J. (1993) A nonlinear mathematical model of pressure preset ventilation: description and limiting values for key outcome variables. *Math. Mod. Meth. Appl. Sci.*, 3, 839-859.
- CROOKE, P. S., MARINI, J. J. & HOTCHKISS, J. R. (2002) Modeling recruitment maneuvers with a variable compliance model for pressure controlled ventilation. J. Theor. Med., 4, 197–207.
- CROTT, S., MASCHERONI, D. et al. (2001) Recruitment and decruitment during acute respiratory failure-A clinical study. Am. J. Respir. Crit. Care Med., 164, 131-140.
- DESHPANDE, N. S. & BARIGOU, M. (2000) The flowof gas-liquid foams in vertical pipes. Chem. Eng. Sci., 55, 4297-4309.
- EICHACKER, P. Q., GERSTENBERGER, E. P. et al. (2002) Meta-analysis of acute lung injury and acute respiratory distress syndrome trials testing low tidal volume. Am. J. Respir. Crit. Care Med., 166, 1510-1514.
- HERNANDEZ, L. A. et al. (1990) Mechanical ventilation increases microvascular permeability in oleic acid-injured lungs. J. Appl. Physiol., 69, 2057–2061.
- HUBMAYR, R. D. (2002) Perspective on lung injury and recruitment: a skeptical look at the opening and collapse story. Am. J. Respir. Crit. Care Med., 165, 1647-1653.
- JEDLINSKA, B., MELLSTROM, A. et al. (2001) Evaluation of splanchnic perfusion and oxygenation during positive end-expiratory pressure ventilation in relation to subcutaneous tissue gases and pH-An experimental study in pigs with oleic acid-induced injury. Eurp. Surg. Res., 33, 237-244.

- MARINI, J. J., CROOKE, P. S. et al. (1989) Determinants and limits of pressure-preset ventilation: a mathematical model of pressure control. J. Appl. Physiol., 67, 1081-1092.
- MARINI, J. J. & CROOKE, P. S. (1993) A general mathematical model for respiratory dynamics relevant to the clinical setting. Am. Rev. Respir. Dis., 147, 14-24.
- MARTYNOWICZ, M. A. et al. (2001) Mechanisms of recruitment in oleic acid-injured lungs. J. Appl. Physiol., 90, 1744-1753.
- MUTCH, W. A. C., HARMS, S. et al. (2000) Biologically variable ventilation increases arterial oxygenation over that seen with positive end-expiratory pressure alone in a porcine model of acute respiratory distress syndrome. Crit. Care Med., 28, 2457–2464.
- NAM, A. J., BROWER, R. G. et al. (2000) Biologically variability in mechanical ventilation rate and tidal volume does not improve oxygenation or lung mechanics in canine oleic acid lung injury. Am. J. Respir. Crit. Care Med., 161, 1797-1840.
- NEUMANN, P., BERGLUND, J. E. et al. (2000) Effects of inverse ratio ventilation and positive end-expiratory pressure in oleic acid-induced injury. Am. J. Respir. Crit. Care Med., 161, 1537-1545.
- NEUMANN, P. & HEDENSTIERNA, G. (2001) Ventilatory support by continuous positive airway pressure breathing improves gas exchange as compared with partial ventilatory support with airway pressure release ventilation. *Anesth. Analgesia*, **92**, 950-958.
- PELOSI, P., GOLDNER, M. et al. (2001) Recruitment and derecruitment during acute respiratory failure-An experimental study. Am. J. Respir. Crit. Care Med., 164, 122-130.
- SAWADA, S., MATSUDA, K. et al. (2002) Effects of partial liquid ventilation on unilateral lung injury in dogs. Chest, 121, 566-572.
- SCARPELLI, E. M. (2003) Review physiology of the alveolar surface network. Com. Bioc. Physiol., 135, 39-104.
- SMITH, R. A., RASANEN, J. O. & DOWNS, J. B. (1991) Flow, pressure, and time modifications. *Contemporary Management in Critical Care: Mechanical Ventilation and Assisted Respiration*, Vol. 1. (A. Grenvik & J. B. Downs, eds). New York: Churchill Livingstone, pp. 15-28.
- STEWART, T. E. (2002) Controversies around lung protective mechanical ventilation (editorial). Am. J. Respir. Crit. Care Med., 166, 1421-1422.
- VAN DER KLOOT, T. E., BLANCH, L. et al. (2000) Recruitment maneuvers in three experimental models of acute lung injury-Effect on lung volume and gas exchange. Am. J. Respir. Crit. Care Med., 161, 1485-1494.
- VAZQUEZ DE ANDA, G. F. & LACHMANN, B. (2001) Review article treatment and prevention of acute respiratory failure: physiological basis. Arch. Med. Res., 32, 91-101.
- WILSON, T. A. et al. (2001) Mechanical of edematous lungs. J. Appl. Physiol., 90, 2088-2098.
- ZHAN, Q. Y., WANG, C. et al. (2001) Efficacy of continuous tracheal gas insufflation in spontaneously breathing canine with acute lung injury. Chin Med. J., 144, 658-660.



Craphs With Small Corounference and Connected Complements

A NUMERICAL STUDY OF BLOOD FLOW PATTERNS IN CORONARY ARTERY BYPASS GRAFTS*

D. POLTEM †, B. WIWATANAPATAPHEE †, P. RUENGSAKULRACH [‡], Y. LENBURY †, M. PUNPOCHA [‡], AND Y.H WU [¶]

Abstract. The control of flow pattern of blood through the grated coronary artery is essential for the success of a bypass surgery. Over the last few decades, extensive studies have been carried out to model many sapects of the coronary artery bypass grafting (CABG). However, due to the complexity of the problem, some physiological and mechanical aspects have still not been fully understood. In this paper, we develop a finite element based on numerical model for the almulation of the flow of blood through the grafted coronary artery and then use the model to study the flow behavior of blood in the right coronary artery for the cases with and without a bypass graft. The effects of bypass graft angle on flow pattern are presented.

1. Introduction. It has been reported that cardiovascular disease is the leading cause of death in developed countries [7, 15]. In recent years, surgical treatments of cardiovascular diseases have been developed rapidly, and coronary artery bypass grafting (CABG) has been widely used for patients with serve coronary artery bypass grafting (CABG) has been widely used for patients with serve coronary artery bypass. A large number of bypass grafts are implanted worldwide each year. However, up to 25% of the grafts fail in one year and up to 50% fail in ten years [16]. Several reasons have been proposed to explain why these grafts clog up or fail [1, 19]. Typical reasons include: (1) improper anastomosis techniques and configuration resulting in an inadequate or overflow of blood through the grafted coronary artery, (2) progression of atheroxclerotic disease of the native coronary artery related to intimal hyperplassis, wall shear stress and progressive risk factors [2, 22]. One of the most important determinants if r a successful bypass surgery is the proper bypass geometry and flow distribution in the neighborhood of the anastomosis.

To understand the flow behavior, extensive studies have been conducted to study the flow patterns of blood through the graft and the native coronary artery. Various flow quantification techniques such as intravacular ultrasound (IVUS) [6], haser Doppler anemometry (LDA) [13], ultrasound Doppler (US) [12]and magnetic resonance imaging (MRI) [14] are commonly used to study arterial hymodynamics. Nowedsys, computational fluid dynamics (CFD) algorithms coupled to realistic 3-D model of such vessel make these data accessible [3]. A number of numerical studies of the blood flow patterns in CABG have also been carried out [8, 9, 10, 11, 18, 20].

The purpose of this paper is to develop a CFD based finite element technique [23] for simulating blood flow in coronary arteries and then uses the technique to study the

⁴Department of Mathematics. Curtin University of Technology, Perth, Australia.

Bangkok 10800, Thalland.

[&]quot;This work was supported by the Thalland Research Fund (TRF) and by the Division of Cardiac Surgery, Heart Institute Saint Louis Hospital and Foundation.

Surgery, Heart Institute Saint Louis Hospital and Foundation. [†]Department of Mathematics, Faculty of Science, Mahidol University, Bangkok 10400, Thalland (acbur**tnah**idol.ac.th).

[‡]The Division of Cardisc Surgery, Heart Institute, Saint Louis Hospital, Bangkok 10120, Thaid.

[‡]Department of Mathematics, Faculty of Science, King Mongkut's Institute of Technology,

flow behavior of blood through the bypass graft and the coronary artery. The effects of varying the anastomesis graft angle on the llow behavior in the native coronary artery are investigated. 2. The Underlying Boundary Value Problem. The blood is assumed as an incompressible Newtonian fluid. The governing equations consist of the continuity equation and the Navier-Stokes equations, which can be expressed in index notation

$$0 = \int_{\mathcal{U}_i} \left(u_{i,j} + u_j u_{i,j} \right) + p_{i,l} - (\mu(u_{i,j} + u_{j,l}))_{i,j} = 0$$

(2.2)

constitute a system of four partial differential equations in terms of four coordinate tively pressure and density of blood; μ is the viscosity of blood. Equations (2.1)-(2.2) where it, denotes the velocity component in the x, direction, p and p denote respecdependent unknown functions $(u_1, u_2, u_3 \text{ and } p)$ for three dimension cases To completely define the flow problem, boundary conditions for the velocity and pressure fields must be specified. For a typical CABG system as shown in Figure 1, the boundary of the computation region consists of four parts, namely the inflow SHIFINCES Of the native artery Io and the bypass graft In, the artery wall In and the outflow boundaries Lexit.

On the inflow surfaces Γ_0 and Γ_n , velocity is set to mean velocity, namely U_{nn} . No-slip condition is applied to the artery wall. The outflow boundaries, I ezes, correspond to

$$-p + \left(\frac{1}{R_e} \frac{\partial H}{\partial H}\right) = 0$$

ber delined by $Re = \frac{eUd}{u}$, U and d denote the average velocity and the diameter of where n is the unit normal vector to the outlet section and Re is the Reynold numinvestigation, respectively.

In summary, the fluid flow problem in CABG is governed by the following boundary

BVP: Find u1, u2, u3 and p such that the field equations (2.1) and (2.2) are satisfied in Ω and all boundary condition are satisfied. 3. A Numerical Algorithm Based on the Finite Element Method. To solve the BVP problem, firstly, the penalty function method is used to weaken the continuity requirement (2.1) by the following equation

$$u_{i,i} = -\delta p_i$$

where 6 is a small positive number. Thus, we obtain the following alternative boundary value problem.

Find $u_{i,i} = 1, 2, 3$ and $p \in H^1(\Omega)$ such that for all ξ^i and $\zeta \in H^1_0$, all the Dirichlet boundary conditions are satisfied and

A NUMERICAL STUDY OF BLOOD FLOW PAITTERNS

(3.1)
$$(u_{i,i},\varsigma) = (-\delta p,\varsigma),$$

(3.2)
$$\left(\frac{\partial u_i}{\partial t}, \xi^i\right) + \left(u_j u_{i,j}, \xi^i\right) - \left(\left(\frac{\mu}{\rho} \left(u_{i,j} + u_{j,i}\right)_{,j}\right), \xi^i\right) + \frac{1}{\rho} \left(p_{,i}, \xi^i\right) = 0$$

where (\cdot,\cdot) denotes the inner product on the square integrable function space $L^2(\Omega), H^1(\Omega)$ is the Sobolev space $W^{1,2}(\Omega)$ with norm $\|\cdot\|_{1,2,\Omega}$ and $H^1_0(\Omega) = \{v \in H^1(\Omega)|v=0 \text{ on the Dirichlet type boundary}\}.$

lem into a finit, dimension subspace. Firstly, we choose an N-dimensional subspace $H_h \subset H^1(\Omega)$ for u_i and the corresponding test function. Let $\{\phi_i\}_{i=1}^N$ be the basis To find the Galerkin numerical solution of the above problem, we pose the probfunctions of H_h , then we have

(3.3)
$$u_j(x,t) \approx (u_j)_h = \sum_{i=1}^N (u_j)_i(t)\phi_i(x)_i$$

$$\xi' \cong \xi_i' = \sum_{i=1}^N \phi_i(x)\xi_i'$$

Secondly, we choose an M-dimensional subspace $H_{eta}\subset H^1(\Omega)$ for p and ς . Let $\{\psi_i\}_{i=1}^N$ be the basis function of H_{β} , then we have

(3.5)
$$p(x,t) = \sum_{i=1}^{M} (p_i)(t)\psi_i(x),$$

(3.6)
$$\zeta = \sum_{i=1}^{M} \psi_i(x) \zeta_i.$$

In principle, H_{β} can be chosen to be the same as H_{λ} . However, our numerical experiments have shown that it is necessary to choose H_{β} to be different from H_{Λ} to By substituting (3.3)-(3.6) and noting that \$\xi^4\$ and \$\xi\$ are arbitrary and using Green's ensure the convergence of the solution to our problem.

 $(\psi_k,\phi_{j,k})u_{ji}=(\delta\psi_k,\psi_l)p_l,$ formula, we have (3.7)

$$(\phi_k,\phi_l)_{il(l)} + \{(\phi_k,u_j\phi_{l,j}) + (v\phi_{k,j},\phi_{l,i})\}_{u_{li}} - \frac{1}{\rho} + \left\{(\phi_{k,l},\psi_l) - \int\limits_{\Gamma \in \mathcal{I}(l)} \phi_k\psi_l n_i d\Gamma\right\}_{p_l}$$

$$(3.8)$$

A NUMERICAL STUDY OF BLOOD FLOW PATTERNS

where $\nu=\frac{\mu}{\rho},$ u_R represents the value of v_R at the t h node of the linite element mesh. The system of equations (3.7) and (3.8) can be written in matrix form as follows

$$(3.9) C^T U = -\delta M_p P,$$

(3.10)
$$M\dot{U} + (\dot{A} + B)U - CP = 0,$$

From (3.10), we have

11)
$$P = -\frac{1}{\delta}M_p^{-1}C^TU$$

which is then used to eliminate the pressure in the momentum equations, and thus

$$(3.12) M\dot{U} + DU =$$

where $D = A + B + \frac{1}{3}CM_p^{-1}C^T$

Using the backward Euler differentiation scheme for a typical time step (t, -th+1), we have from system (3.12) that

$$\left(\frac{M}{\Delta t_{\rm n}} + D\right) U_{\rm n+1} = \frac{M}{\Delta t_{\rm n}} U_{\rm n}$$

which is nonlinear because D depends on U_{n+1} . To deal with this nonlinearity for an iterative solution of (3.13), we use the iterative update

$$\left(\frac{M}{\Delta t_n} + D_{n+1}^i\right) U_{n+1}^i = \frac{M}{\Delta t_n} U_n$$

where the superscript i denotes evaluation at the ith iteration step. Therefore, in a typical time step $(t_n \to t_{n+1})$, starting from $U_{n+1}^0 = U_n$, we determine U_{n+1} by solving system (3.14) repeatedly until $||U_{n+1}^{l+1} - U_{n+1}^{l}|| < T$ olerance. By repeatedly using above procedure for n=0,1,2,, we can determine the state U of the system at $t_0,t_1,t_2,...$ If the norm $\|U_{n+1}-U_{n+1}\|$ is sufficiently small, then the system approaches the so-called steady state.

shown in Figure 2, represents the 50% stenosed right coronary artery. Diameter of the native artery varies from 0.125 cm to 0.384 cm and the length of investigation is 10,525 cm. Using the flow rate Q(t) reported by Bertolotii et.al (2001) [5] as shown Flow simulations were conducted under a typical physiological condition: a heart fate of 84 beat per minute. The fluid properties are typical of human blood with a viscosity $3 \times 10^{-2} \text{ gcm}^{-1}\text{s}^{-1}$ and a density of 1.06 gcm⁻³ [21]. The computation region, as in Figure 3, the mean flow rate is estimated by the following formula

$$Q_{\alpha\nu\rho} = \frac{1}{T_c} \int_0^{T_c} Q(t) dt$$

where T_o is the period of each cycle of 0.714 s, Qavg and Q(t) denote respectively the mean flow rate and the translent flow rate. The mean flow velocity can be approximated as 20.13 cm/s. Various angles of bypass graft were used to investigate the effect of graft angles on blood flow patterns in native coronary artery. We simulate the blood flow through the bypassed right coronary artery in twodimension. The mesh as shown in Figure 4 consists of 8257 nodes and 15006 elements. To get flow patterns in successive cycles, we consider 1.4 cycles in the computation and each cycle is divided into 200 time steps with step size 3.57 ms.

tomosis leads to higher velocity in the neighborhood of the proximal and immediate distal parts in comparison to the one with higher degree anastomosis. Figure 6 shows that there exists turbulent retrograde flow along the vessel wall in the neighborhood of the heel and toe parts. The velocity of the recirculating flow tands to decrease with the increase of the anastomosis angles. Compared with other angles, the configuration with a 10 degree angle of anastomosis produces the highest flow velocity at the far The results as shown in Figure 5 indicate that the bypass grafting with a $10^{
m o}$ anasdistal part of the native artery as abown in Figure 7.

the mean flow in the far distal coronary artery has a quadratic relationship with the right coronary artery bypass grafting is presented based on the Bubnov-Galerkin Finite Element formulation. The two-dimensional regional flow is calculated. As the blood flows from a graft into the native coronary artery, it hits the jet flow from the native artery. The results indicate that the residual flow issued from the stenosed artery creates a jet flow, which intends to decrease after bypass operation. The study shows that for a graft with the same diameter as the native artery, the mean flow velocity in the neighborhood of the far distal part of the native artery is larger than that in the proximal part of the native artery. The recirculation zone occurs in the neighborhood of the toe and heel of the graft for all graft angles. It is also found that graft angless. Proper choice of the diameter of the graft might improve the balance of inflow and outflow in the coronary artery. It shall be addressed that to improve the accuracy of results, the two-dimensional blood flow study has to be extended to 4. Conclusions. A numerical model of blood flow patterns in the half stenowed pulsatile inflow, three-dimensional realistic domain.

Acknowledgments. The authors are grateful to the Thailand Research Fund (TRF) for the support of this research and also wish to thank the Division of Cardinc Surgery, Heart Institute Saint Louis Hospital and Foundation for the information.

REFERENCES

[1] H.B. Barner, Techniques of myocardial revuscularization, In: Edmunds LH Jr (vd) Cardine surgery in the adult. McGrnw Hill, New York, (1997), pp.

POLTEM, WIWATANAPATAPHEE, RUENGMAKULRAGH, LENBURY, PUNPOGHA AND WU

._

- II.S -BASSIOUNY, WHITE S, GLAGOV S, CHOI E, GIDDENS DP, ZAILINS CK, Anastomotic intimal hyperplasia and medial thickening in autogenous vein graft, Sugery, 15(1992), pp. 708-17.
 - BERTHIER, R. BOUZERAR, C. LEGALLAIS, Blood flow pattern in an anatomicully realistic coronary vessel: influence of three different reconstruction methods, J Biomech, 35(2002), pp. 1347-56. Ė E
- BERTOLOTTI, V. DEPLANO, Three-dimensional numerical simulations of flow through a stenosed coronary bypass, J Blomech, 33(2002), pp. 1011-22. j
- BERTOLOTTI, DEPLANO V, FUSERI J, DUPOUY P, Numerical and experimental models of post-operative realistic flows in stenosed coronary bypasses, J Biomech, 45(2001), pp. 1049-64. : ::
 - ments in humans. Feasibility, reproducibility, and hemodynamic flow versus C.R., WIJNS, W., Simultaneous coronary artery presure and flow measure-BRUYNE, B., BARTUNEK, J., SYS, S.U., PIJLS, N.H.J., HEYNDRICKX, presure stope index, and fractional flow reserve, Circulation, 94(1996), pp. Ö :=.
- (7) CARO, C.G., FITZ-GERALD, J.M., SCLIROTER, R.C, Atheroma and arterial wall shear; observation, correlation and proposal of a shear dependent mass transfer mechanism for stherogenesis, Proc. Roy. Soc. B, 177(1971), pp. 109-
- S. CHAKRAVARTY, P.K. MANDAL, Two-dimensional blood flow through tapered arteries under stenotic conditions, Internat. J. Non-lineur Mech, 35(2000), 2
- 191 TU CHENG, MICHEL DEVILLE, Pulsatile flow of non-Newtonian fluid through arterial stenosis, J Biomech, 29(1996), pp. 899-908.
- 10 J.S. Cole, J.K. Warrenson, M.J.G. O'Reilly, Numerical investigation of heamodynamics at a palched arterial bypass anastomosis, Medical Engineerия & Physics. 24(2002), pp. 393-401.
 - D.Y. FEI, J.D. THOMAS, S.E. RITTGERS, The effect of angle and flow rate upon hemodynamics in distal vascular graft anastomoses; a numerical model study, J Biomech Eng, 116(1994), pp. 331-6. ---
 - [12] L. ILATLE, B.P. ANGELSEN, Doppler Ultrasound in Cardiology, Lea and Felbiger, Philadelphia, PA. 1985.
- 13 D. LEUPHECHT S. MORAVEC, Pubaille flow of non-Newtonian fluid in distensible models of human arteries, Biorheology, 21(1984), pp. 571-86.
- [14] G.L. NAYLER, D.N. FIRMIN, D.B. LONGMORE, Blood flow imaging by cine magnetic resonance imaging, Journal of Computer Assisted Tomography,
- [15] Organisation Mondiale de la Sante (OMS). Annual Report, 1999. [16] Y. Papahanilaou, D.J. Doorly, S.J. Sherwin, The influence of out-of plane geometry on pulsatile flow within a distal end-to-side anastomosis, J Biomech 35(2002), pp. 1255-39.
- RENE, R. GERHARD, B.S. MARKUS, L. DIETER, P. KARL, B. PETER; Hemodynamics in the carotid artery bifurcation: a comparison between numerical simulations and in vitro MRI measurements, J Biomech, 33(2002). m 17]
 - 18, C. Ross Etheir, D.A. Steinman, X. Zhang, S.R. Karpik, M. Ojha, Flow waveform effects on end-to-side anastomotic flow patterns, J Biomech, 31(1998), pp.

A NUMERICAL STUDY OF BLOOD FLOW PATTERNS

- T. SEKI, KITAMURA S KAWACHI K, A quantitative study of postoperative luminal narrowing of the internal thoracic artery graft in the coronary bypass surgery, J Thorne Cardiovase Surg, 104(1992), pp. 1532. 13
 - [20] M.H SONG, MASARU SATO, YUICHI UEDA, Three-dimensional Simulation of coronary artery bypass grafting with the use of computational fluid dynamics
 - [21] D. TANG, C. YANG, S. KOBAYASHI, KU DIN, Steady flow and wall compres-Surgery Today, 30(2002), pp. 993-98.
 - sion in stenotic arteries: a three-dimensional thick-wall model with fluid-wall interactions, J Biomech Eng, 123(2001), pp. 548-57. [22]
 - K.C. WATTS, A.E. MARBLE, S.N. SARWAL, C.E. KINLEY, J. WATTON, M.A. MASON, Simulation of coronary artery revascularization, J Biomech, 19(1986), pp. 491-99.
- B. WIWATANAPATAPHEE, Mathematical modeling of fluid flow and heat transfer the continuous steel casting, Ph.D Thesis. (1998), pp. 107-131 [23]

A COMPARISON OF THE AGE DISTRIBUTIONS IN THE DENGUE HEMORRHAGIC FEVER EPIDEMICS IN SANTIAGO DE CUBA (1997) AND THAILAND (1998)

P Pongsumpun¹, S Yoksan² and IM Tang^{2,3}

¹Department of Mathematics; ³Department of Physics, Faculty of Science, Mahidol University, Bangkok 10400, Thailand; ²Center for Vaccine Development, Institute of Science and Technology for Research and Development, Mahidol University, Nakhon Pathom 71730, Thailand

Abstract. The age profiles of the infected populations of two dengue hemorrhagic fever (DHF) epidemics, the 1997 epidemic, in Santiago de Cuba and the 1998 epidemic in Thailand, are compared. Using an age-structured model of disease transmission, the dependence of the forces of infection on age was determined for each epidemic. The difference in the behavior of the two epidemics and the role of primary and secondary infection in the development of DHF are discussed.

INTRODUCTION

Dengue hemorrhagic fever (DHF) is an emerging viral disease that is spreading throughout the tropics. Since its first appearance, in the Philippines in 1953, DHF has become the most important arthropod-borne viral disease of humans (WHO, 1997). It has been estimated that there are between 50 and 100 million cases of dengué fever (DF) a year; more than 250,000 annual cases of dengue hemorrhagic fever (DHF) result in some 10,000 infant deaths. Classic dengue fever is a disease of older children and adults; DHF, on the other hand, is primarily a disease of children under the age ... 15 (Gubler, 1998). DHF differs from DF: plasma leakage is seen in DHF. Both diseases are caused by one of four serotypes of the dengue virus, (DEN1, DEN2, DEN3, and DEN4) which belongs to the genus Flavivirus, family Flaviviridae.

Because two of the mosquito vectors, Aedes aegypti and Aedes albopictus, exist in the Americas, DF has become endemic in the New World (Pan American Health Organization, 1994). The first severe outbreak of DHF

Correspondence: IM Tang, Department of Physics, Faculty of Science, Mahidol University, Bangkok 10400, Thailand.

E-mail: scimt@mahidol.ac.th

in the Americas occurred in 1981 in Cuba (Guzman et al. 1990) and gave rise to 334,203 DF cases, 10,313 documented DHF cases, and 158 deaths. The serotype responsible for the epidemic was DEN2. An earlier epidemic of mild classic dengue fever, which occurred between 1977 and 1979, was caused by a different strain (DEN1). During this epidemic, the sera of 44.5% of a random sample of 2,000 people contained DEN1 virus antibodies (HI; hemagglutination inhibition). Strict infection control measures adopted after the 1981 epidemic lead to the disappearance of DHF from Cuba for the next sixteen years. A localized outbreak of DHF occurred in Santiago de Cuba in 1997 (Kouri et al. 1998; Guzman et al, 2000). The culprit was the DEN2 virus.

To get a better understanding of the transmission of this disease, we compared the DHF epidemic that occurred in Santiago de Cuba in 1997 with the one that occurred in Thailand in 1998. We were interested in the age distribution of those infected during the two epidemics. Most literature on DHF mentions that the disease affects mainly those under the age of 16; Guzman et al (1997) noted that almost no-one under the age of 17 became sick with DHF (Fig 1a). This is quite different from the age pattern seen in epidemics, which occur in countries in which the disease is fully established. Fig 1b shows the age distribution in

one province of Thailand during the 1998 epidemic (Ministry of Public Health, 1998).

MATERIALS AND METHODS

Before a discussion of the differences between the two distributions can be held, the age distribution of the forces of infection in the 1997 DHF epidemic in Santiago de Cuba must be determined. The force of the DHF infection in Thailand during the 1998 epidemic has already been established. Pongsumpun and Tang (2001) who showed that the percentage of infected people (I) in the i-th age cohort (I) is

$$I_{i} = \frac{\alpha}{\alpha + r + \mu_{h}} I_{i-1} + \frac{\beta^{h} i I_{v}}{\alpha + r + \mu_{h}} S_{i}$$

for i = 2,...N-1 (i)

with

$$I_{l} = \frac{\beta^{h} II_{v}}{\alpha + r + \mu_{h}} S_{l}$$
 (ii)

$$S_i = \frac{\alpha}{\beta^h i I_v + \alpha + \lambda} S_{i-1}$$
 (iii)

and

$$S_{i} = \frac{\lambda}{\beta^{h} II_{v} + \alpha + \lambda}$$
 (iv)

In the above, β_i^h is the transition rate for the virus to be transmitted to humans by mosquitos (the force of infection); α is the rate at which one cohort age into the next; r is the recovery rate; λ is the birth rate; μ_h is the death rate of the human population; and I_{ν} is the number of infected mosquitos divided by their total number.

RESULTS AND DISCUSSION

The forces of the DHF infections can be determined by fitting the incidence rates given

in Fig 1a to equations (i) to (iv) by varying the values of β^h ; this yields the values of β^h ; that are shown in Fig 2. The behaviors of the forces of infection in the two epidemics look the same, ie, an initial increase followed by a drop to a nearly constant force of infection, except that the initial increase is shifted 16 years in the case of the Santiago de Cuba epidemic.

To understand why this happens and why the age distributions shown in Figs 1a and 1b are as they are, two theories of the pathogenesis of dengue hemorrhagic fever must be considered. The first, more commonly accepted theory, is the immune enhancement or secondary-infection hypothesis (Halstead, 1988). According to this hypothesis, the pre-existing heterologous dengue antibody in an infected person recognizes a novel dengue virus and forms an antigen-antibody complex, which then bonds the virus to the membrane of a leukocyte. Because the antibody is heterologous. the virus is not neutralized and remains free to replicate inside the leukocyte. These infected cells then produce and secrete vasoactive mediators in response to the infection; these mediators cause an increase in vascular permeability, leading to hypovolemia and shock.

In the second theory, the dengue virus mutates as it replicates in the human and/or the mosquito. Some of these mutations lead to more virulent viruses: these viruses causing DHF. Because a pre-existing antibody is implicated in the first theory, the infection causing DHF must be a secondary one. In the second theory, no pre-existing antibody is required: primary dengue infection can cause DHF.

43

If the secondary-infection hypothesis is correct, the paucity of DHF-infected children in the 1997 epidemic in Cuba is under stand able: no-one under the age of 16 would have had pre-existing dengue virus antibodies in his blood because he would have been born after the 1981 epidemic. Of the individuals under the age of 16 years who were tested for dengue antibodies in Santiago de Cuba. only 2% had

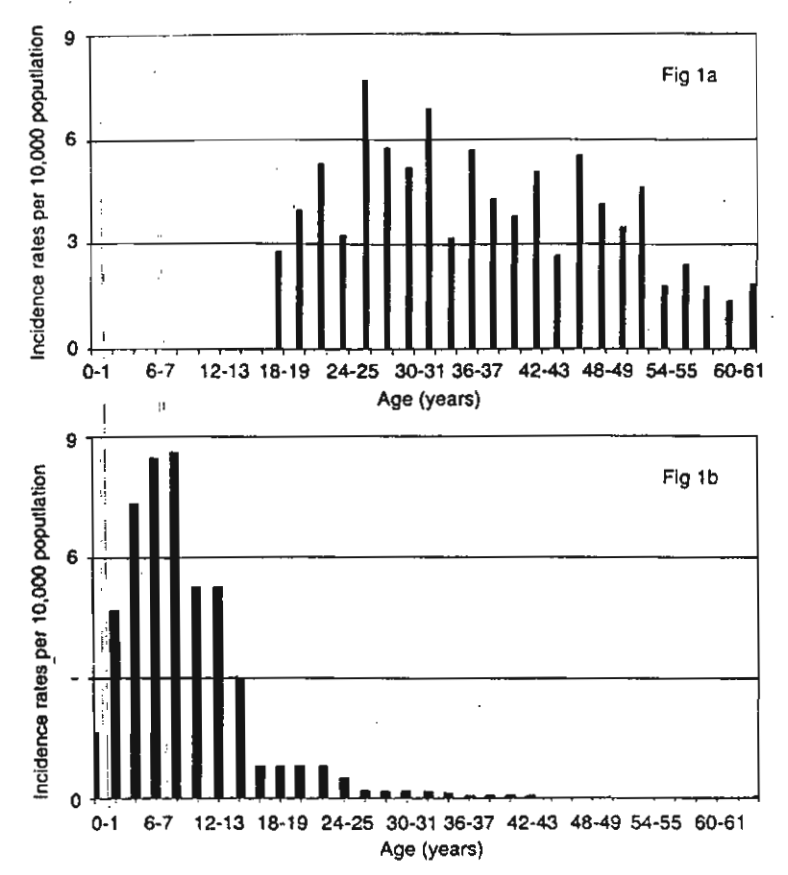


Fig 1-Age distribution of dengue hemorrhagic fever. (1a) Age distribution of the 1997 epidemic in Santiago de Cuba.

(Data from Guzman et al, 2000). (1b) Age distribution of the 1998 epidemic in Mukdahan Province, Thailand (Data from Ministry of Public Health, 1998).

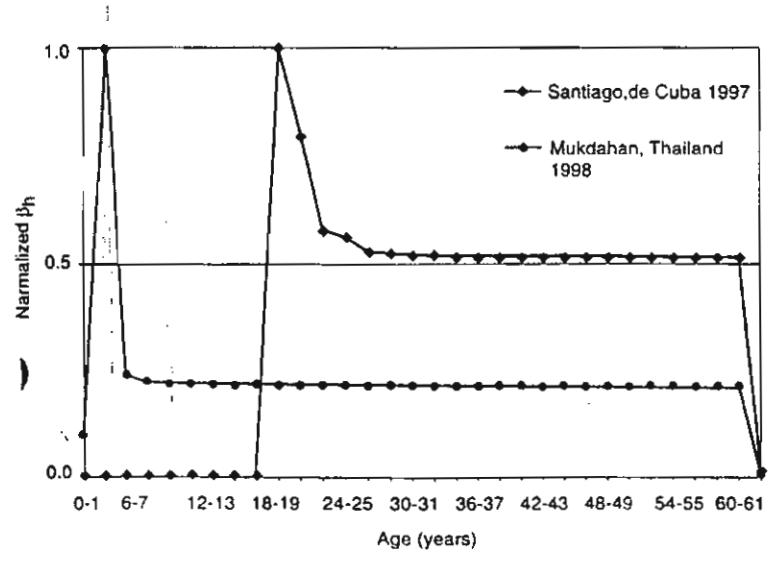


Fig 2-Forces of infection in the two epidemics. Forces of infection in Santiago de Cuba are denoted by (♠); forces of infections in Mukdahan Province, Thailand, are denoted by (♠). Values obtained by fitting equations (i) to (iv) to the incidence rates presented in Figs 1a and 1b.

the neutralizing antibodies to DEN2 and none had the antibodies to DEN1 (Guzman et al, 2000). Serological tests showed that the dengue infections in 98% of the DHF/DSS cases were secondary. In a study of the 1994 epidemic in Thailand (Vaughn et al, 1997) it was found that while 93% (56 of 60) of the children with DHF were experiencing a secondary infection, only 4% were experiencing a primary infection. Vaughn et al (1997) also showed that the viremia was correlated with the body temperature of the patient; they were able to isolate the virus in 59 of 60 DHF patients, who were in the early febrile stage.

However, not all the evidence supports the secondary-infection hypothesis. During the 1996-1997 epidemic in Belem, Brazil (Travassos de Rosa et al. 2000) none of the 24 individuals, in whom the DEN2 virus was isolated and who were previously infected with the DEN1 virus, developed DHF. tional evidence was obtained about the 1998 epidemic in Thailand from the serological records of the Department of Pediatrics, Siriraj Hospital (the largest hospital in Thailand). The pediatric ward at Siriraj Hospital admitted 316 children suffering from DHF in 1998. Hemagglutination inhibition assay (HAI) and IgM/IgG capture enzyme-linked immunosorbent assay were conducted for serum samples from all the patients. The dengue virus (49 DEN1, 29 DEN2, 41 DEN3, and 1 DEN4) was isolated in 120 of these patients.

We are interested in this subgroup. Vaughn et al (1997) have suggested that the following criteria be used to determine whether an infection is primary or secondary. Primary infection: HAI reciprocal titers ≤ 640; IgM to IgG ratio > 1.8. Secondary infection: HAI reciprocal titers > 1,280; IgM to IgG ratio < 1.8. Applying these criteria to the

serological results, 56 of the 120 DHF patients were experiencing a primary infection by the HAI criterion; 27 were experiencing a primary infection by the IgM/G criterion; and 13 satisfied both criteria. Among this group of 13 children, there were 7 cases in which the primary infection was due to DEN1 virus; 3 cases were due to DEN2 virus, and 3 were due to the DEN3 virus. This would appear to contradict the findings from the 1994 Thai epidemic, in which only 4% of DHF cases were the results of primary infection. We examined the records of Siriraj Hospital for the year 1999. One hundred and thirty-seven children suffering from DHF were admitted to the pediatric ward that year. The dengue virus was isolated in 31 of these patients, none of whom ...d a primary infection based on both tests. It appears that the DHF epidemics in Thailand during 1994 and 1999 differed from the 1998 epidemic in terms of the primary/secondary cause of infection. The reason for this difference is not clear. It is interesting to note that epidemics in Thailand peak every three years (Hay et al, 2001): 1998 was a peak year, while 1994 and 1999 were not. We are now studying this phenomenon to see whether it is of relevance to the problem of primary/secondary infection.

ACKNOWLEDGEMENTS

P Pongsumpun would like to thank the Thailand Research Fund for a Royal Golden Jubilee PhD Scholarship (contract PHD 154/2543). The authors would like to thank the Serological Laboratory, Siriraj Hospital, and the Ministry of Public Health, Thailand for the data used in this study.

REFERENCES

- Gubler DJ. Dengue and dengue hemorrhagic fever. Clin Microbiol Rev 1998; 11: 480-91.
- Guzman MG, Kouri GP, Bravo J, et al. Dengue hemorrhagic fever in Cuba, 1981: A retrospective seroepidemiologic study. Am J Trop Med Hyg 1990; 42: 179-84.
- Guzman MG, Kouri GP, Valdes L, et al. Epidemiologic studies on dengue in Santiago de Cuba, 1997. Am J Epidemiol 2000; 152: 793-9.
- Halstead SB. Pathogenesis of dengue: challenges to molecular biology. Science 1988; 239: 476-81.
- Hay SI, Mymers MF, Burke DS, et al. Etiology of interepidemic periods of mosquito-borne disease. PNAS 2001; 97: 9335-9.
- Kouri G, Guzman MG, Aldes L, et al. Reemergence of dengue in Cuba: A 1997 epidemic in Santiago de Cuba. Emerg Infect Dis 1998; 4: 87-92.
- Ministry of Public Health, Thailand, Annual Epidemiological Surveillance Report (1992-8). Division of Epidemiology, Ministry of Public Health, Thailand, 1998.
- Pan American Health Organization. Dengue and dengue hemorrhagic fever in the Americas: guidelines for prevention and control. Washington DC: PAHO. 1994; 548.
- Pongsumpun P, Tang IM. A realistic age structured transmission model for dengue hemorrhagic fever in Thailand. Southeast Asian J Trop Med Public Health 2001; 32: 336-40.
- Travassos da Rosa APA, Vasconcelos PFC, Travassos da Rosa ES, et al. Dengue epidemic in Belem, Para, Brazil, 1996-97. Emerg Infect Dis 2000; 6: 298-301.
- Vaughn DW, Green S, Kalayanarooj S, et al. Dengue in the early febrile phase: Viremia and antibody responses. J Infect Dis 1997; 176: 322-30.
- World Health Organization. Dengue hemorrhagic fever: diagnosis, treatment, prevention and control, 2nd ed. 1997.

AGE STRUCTURE IN A MODEL FOR THE TRANSMISSION OF DENGUE HAEMORRHAGIC FEVER IN THAILAND

P. Pongsumpun 1,a, Y.Lenbury land I.M.Tang 2,b

Department of Mathematics and ² Department of Physics
Faculty of Science, Mahidol University, Rama 6 Rd., Bangkok 10400, Thailand

² Institute of Science & Technology for Research & Development Salaya Campus, Mahidol University, Nakorn Pathom 71730, Thailand

a g4236738@student.mahidol.ac.th and b scimt@mahidol.ac.th

Abstract

The influence of age structure in the human population in the Susceptible-Infected-Recovered (SIR) model used to describe the transmission of Dengue Haemorrhagic Fever (DHF) is studied. The human population is separated into an adult class and juvenile class with only the juveniles being susceptible to infection by the disease. A new expression for the basic reproduction rate is obtained. It is found that age structure reduces the periods of oscillations in the susceptible human population, infected human population and infected mosquito population and the tightness of the spiraling into the endemic equilibrium state.

Key words and phrases: Dengue haemorrhagic fever, Age structure, SIR model, Endemic equilibrium, Local stability.

1 Introduction

Mathematical modeling of disease transmission has a long history. In 1911, an epidemiology model for malaria transmission was developed by Ross [1]. MacDonald [2] later added a layer of biological realism to the model by providing careful interpretation and estimation of the parameter, which should go into the model. McKenzie [3] has pointed out that the utility of a model depends not as much on how well a mathematical job has been accomplished but how on well a particular question has been translated. One is interested in disease transmission, it is imperative that the model describes as closely as possible the characteristics of the disease being transmitted. In this paper, we are interested in the transmission of dengue haemorrhagic fever (DHF).

Dengue Haemorrhagic fever is one of the emerging viral diseases spreading throughout the tropical regions of the world. From its first appearance in the Philippines in 1953, it has become the most important arthropod-borne viral disease of humans [4]. It has been estimated that there are between 50 and 100 million cases a year, with approximately 10,000 infant deaths due to this disease. Its emergence is associated with the rapid urbanization occurring in the developing countries. Because two of the transmitting vectors, the Aedes aegypti and Aedes albopictus mosquitoes, exist in the Americas, it has been possible for the disease and its rather benign precursor, dengue fever (DF), to become endemic in the New World [5]. The first

AGE STRUCTURE IN A MODEL FOR THE TRANSMISSION OF DENGUE

severe outbreak of DHF in the Americas occurred in 1981 in Cuba with 116,000 hospitalized patients, 34,000 documented DHF cases and 158 deaths. Important outbreaks of DHF have also occurred in Mexico[6].

In hopes of understanding the mechanics that allow the invasion and persistence of a serotype of the dengue virus in a region, Esteva and Vargas [7-9] introduced a mathematical model to provide a qualitative assessment for the problem. The model they used is based on the Susceptible Infected-Recovered (SIR) model often used to model the dynamics of transmission of some diseases. They showed that the endemic state was globally stable whenever a parameter R_0 called the basic reproduction number is greater than one. Application of an ultra low volume (ULV) amount of insecticides (the standard method used to control the spread of dengue fever and other arthropod-borne disease) could reduce the value of R_0 to below one. The value of R_0 would return to the above one value once the application is stopped and since the endemic state is globally stable, the disease would return. Therefore the eradication program would have to be a continuing one.

In the SIR model used Esteva and Vargas, no age structure was incorporated into the models. While the lack of an age structure may be appropriate for describing the 1981 DHF epidemic in Cuba [10] and the DHF outbreak in Santiago de Cuba in 1997 [11], it is not appropriate for Thailand. Most DHF cases in Thailand occur in children less than 15 years old. In figure 1, we show the age distribution of the incidence rates in one province in Thailand during the 1998 DHF epidemic [12]. Feng and Velasco-Hernandez [13] pointed to the need of a model that incorporates age structure into the dengue population dynamics. It is the purpose of this paper to report on a DHF transmission model, which includes an age structure in the human population. Central to any discussion of any population growth is the basic reproduction rate or number. The basic reproduction rate or number. The basic reproduction is intrinsically capable of producing. The inclusion of an age structure leads to a new expression for this number. This is done in section 3.

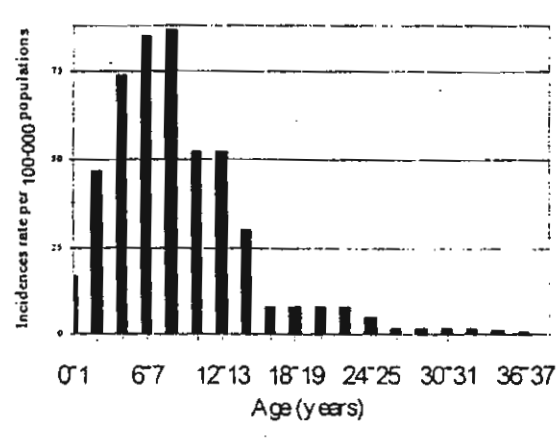


Figure 1. Age distribution of the 1998 Dengue Fever incidence rates in Mukdahan, a province in Central Thailand.

2 Mathematical Model

The simplest way to incorporate an age structure into a disease in which only the children are susceptible to the disease is to divide up the human population into two categories,

!

transmission of the dengue virus to the mosquito from an infected juvenile. $oldsymbol{eta_{
m V}}$ is the transmission probability of dengue virus from an infected juvenile to the mosquito. Introducing the normalized parameters $S = S'/N_T$, $I = I'/N_T$, $R = R'/N_T$, $A = A'/N_T$, $S_v = S_v'/(B/\dot{\mu}_V)$ and $I_v = I_v'/(B/\mu_V)$, equations (1a) to (2b) reduce to

$$\frac{dS}{dt} = \lambda' - \gamma_h I_v S - (\mu_h + \delta) S \qquad , \qquad (3a)$$

$$\frac{dI}{dt} = \gamma_h SI_v - (\mu_h + \delta + r)I \qquad , \qquad (3b)$$

$$\frac{dR}{dt} = rI - (\mu_h + \delta)R \tag{3c}$$

$$\frac{\mathrm{d}l_{\mathrm{V}}}{\mathrm{d}t} = \gamma_{\mathrm{V}} (1 - l_{\mathrm{V}}) l_{\mathrm{V}} - \mu_{\mathrm{V}} l_{\mathrm{V}} \tag{3d}$$

where

$$\gamma_h = \frac{b \beta_h (B / \mu_V)}{N_T + m} \tag{4a}$$

and

$$\gamma_{V} = \frac{b \beta_{V} N_{T}}{N_{T} + m} \tag{4b}$$

The dynamical equations for A and S_V are not needed since S + I + R + A = I and $S_V + I_V =$ 1. The requirement that N_T be a constant leads to the condition that the birth rate, λ is equal to the death rate, μ_h .

2.1 Equilibrium States

The equilibrium states are obtained by setting the RHS of equations (3a) to (3d) to zero. Doing this, we get two equilibrium states, the disease free equilibrium state, $E_0 = (S, 0, 0, 0)$ where

$$S = \frac{\mu_h}{\mu_h + \delta} \tag{5}$$

and the endemic equilibrium state, $E_1 = (S^{\bullet}, I^{\bullet}, R^{\bullet}, I_{V}^{\bullet})$ where

$$S = \frac{\gamma_h + \mu_h X_0}{X_0 (\gamma_h + \mu_h M)}$$
 (6a)

$$I \cdot = \frac{\mu_{V} \mu_{h} (X_{0} - M)}{\gamma_{V} (\gamma_{h} + \mu_{h} M)}$$
 (6b)

$$R = \frac{\mu_{V} \Gamma(X_{0} - M)}{\mu_{V} M(\mu_{D} + \mu_{D} M)}$$
 (6c)

and

$$I_{V} = \frac{\mu_{h} (X_{0} - M)}{(\gamma_{h} + \mu_{h} X_{0})}$$
 (6d)

with

$$M = \frac{\mu_h + \delta}{\mu_h} \tag{7a}$$

and

$$X_0 = \frac{\gamma_h \gamma_v}{\mu_v (\mu_h + \delta + r)} \tag{7b}$$

2.2 Local Asymptotical Stability

The local stability of an equilibrium state is determined from the Jacobian (gradient) matrix of the RHS of the set of differential equations evaluated at the equilibrium state.

2.2.1 Disease Free State

g

For the system defined by equations (3a) to (3d), the Jacobian matrix evaluated at E_0 is the 4×4 matrix given by

$$\begin{pmatrix}
-(\mu_{h} + \delta) & 0 & 0 & -\gamma_{h} / M \\
0 & -(\mu_{h} + \delta + r) & 0 & \gamma_{h} / M \\
0 & r & -(\mu_{h} + \delta) & 0 \\
0 & \gamma_{V} & 0 & -\mu_{V}
\end{pmatrix}$$
(8)

Diagonalizing this matrix, yields the following characteristic equation;

$$(\lambda + \mu_h + \delta)^2 \left\{ \lambda^2 + (M\mu_h + r + \mu_V)\lambda + \mu_V(M\mu_h + r) \left(1 - \frac{X_0}{M} \right) \right\} = 0$$
 (9)

The eigenvalues are

$$\lambda_{1,2} = -(\mu_{\rm h} + \delta)$$

and

$$\lambda_{3,4} = \frac{-(\mu_h + \delta + r + \mu_v) \pm \sqrt{((M\mu_h + r) - \mu_v)^2 + 4\mu_v (M\mu_h + r) \frac{X_0}{M}}}{2}$$
(10)

For $X_0 < M$, the square root will be less than $(\mu_h + \delta + r + \mu_V)$. This means that all the eigenvalues will be negative; leading to the disease free state being locally asymptotically stable.

2.2.2 Endemic Disease State

The characteristic equation for the Jacobian matrix evaluated at the endemic equilibrium state, given by equations (6a) - (6d), is

$$f(\lambda + \mu_H + \delta)(\lambda^3 + A\lambda^2 + B\lambda + C) = 0$$
 (11)

where

$$A = \frac{\mu_{v}(\gamma_{h} + \mu_{h}X_{0})}{\gamma_{h} + \mu_{h}M} + \frac{\mu_{h}X_{0}(\gamma_{h} + \mu_{h}M)}{\gamma_{h} + \mu_{h}X_{0}} + \frac{\gamma_{h}\gamma_{v}}{\mu_{v}X_{0}}, \qquad (12)$$

$$B = \frac{\mu_{h} \gamma_{v} \gamma_{h} (X_{0} - M)}{X_{0} (\gamma_{h} + \mu_{h} M)} + \frac{\mu_{h} (\gamma_{h} + \mu_{h} M) (\mu_{v}^{2} X_{0} + \gamma_{v} \gamma_{h})}{\mu_{v} (\gamma_{h} + \mu_{h} X_{0})} + \left(\frac{\mu_{h} X_{0} (\gamma_{h} + \mu_{h} M)}{(\gamma_{h} + \mu_{h} X_{0})}\right) \left(\frac{\mu_{h} \mu_{v} (X_{0} - M)}{(\gamma_{h} + \mu_{h} M)}\right)$$
(13)

and

$$C = \mu_h \gamma_h \gamma_v \left(1 - \frac{M}{X_0} \right). \tag{14}$$

The real parts of the eigenvalues are negative when the coefficients A,B and C satisfy the Routh-Hurwitz criteria, [7] i.e.,

i.
$$A > 0$$
ii. $C > 0$ (15)

and

Looking at equations (12) to (14), we see that conditions i. is always satisfied. Conditions ii. and iii. are satisfied when $X_0 > M$. [To see that condition iii. is satisfied when $X_0 > M$, we note that the cross product AB will be the sum of positive terms. Given the sum of positive numbers is greater than any individual number, we have $AB > \mu_h \{ \mu_v^2 X_0 + \gamma_h \gamma_v \}$ (this being the product of the first term in A and the second term in B). Dropping $\mu_v^2 X_0$ in the bracket, we see that $\mu_h \gamma_h \gamma_V$ is larger than $\mu_h \gamma_h \gamma_V (1-M/X_0)$, which is C. We thus have AB > C.] This shows that if $X_0 > M$, the real parts of all the eigenvalues of the Jacobian evaluated at the endemic state are negative. Thus the equilibrium state $E_2(S^*, I^*, R^*, I_V)$ given by equations (6a) - (6d) is a locally asymptotically stable state.

3 Discussion

3.1 Basic Reproduction number

For a disease to be capable of invading and establishing itself in a host population, the basic reproduction number R_0 must be greater than one. If $R_0 < 1$, then every successive generation will diminish in size until its number approaches zero. The basic reproduction number for a particular growth can be determined by direct observation of the growth pattern. If t_d is the first doubling time of the epidemic in a human population, then

$$R_0 = \left[\frac{\ln 2}{(\mu + \delta)t_d} + 1 \right]$$

where μ and δ refer to the inverse life time and recovery time of the human. The average reproduction number for the 1990-91 dengue fever epidemic in twelve cities in Brazil was 2.03 [14]. This number means that each infective person infected 2.03 other people. Koopman et al.,[15] found the number to be 1.33 for the dengue fever epidemic in Mexico in the same year.

The different models for disease transmission have yielded expression for the basic reproduction number. These expressions have provided insights into the control of the various diseases. One of the first expressions obtained was

$$R_0 = \frac{b^2 \beta_h \beta_v m}{\mu \gamma}$$
 (16)

where m is the ratio between the mosquito population and the human population. Based on the epidemiological data, Molineaux and Gramiccia [16] estimated R_0 to be 80 for the malaria epidemic in northern Nigeria. The implication of this (each infective person infects 80 other people) points to possible shortcoming of the model used model the transmission of malaria. We note that for dengue fever, R_0 is close to 2. It was pointed out by MacDonald that the malaria transmission model did not take into account an incubation period during which the malaria parasite develops inside the mosquito and during which the mosquito is not infections. Taking this period into account, MacDonald obtained a new expression for the basic reproduction number

$$R_0 = \frac{b^2 \beta_h \beta_v m}{\mu \gamma} e^{-\mu r}$$
 (17)

where μ and τ are the inverse life time of the mosquito and the incubation period of the malaria parasite in the mosquito. Equation (17) points to the fact that if the incubation period is longer than the life expectancy of the mosquito, the disease will not be established since the mosquito will die before it becomes infectious. The appearance of an exponential factor containing the life expectancy of the mosquito has led to the changes in the strategy of control malaria, exterminate the mosquito during its adult state and not in it's the larva stage.

Looking at the conditions (given in sections 2.2.1 and 2.2.2), which made the disease free state or the endemic state, the stable equilibrium state, we obtain the following conditions

$$\frac{b^2 \beta_v \beta_h \mu_h N_T (B/\mu_v)}{\mu_v (N_T + m)^2 (\mu_h + \delta + r) (\mu_h + \delta)} < 1$$

for the equilibrium state to be the disease free state. If however,

$$\frac{b^{2}\beta_{V}\beta_{h}\mu_{h}N_{T}(B/\mu_{V})}{\mu_{V}(N_{T}+m)^{2}(\mu_{h}+\delta+\Gamma)(\mu_{h}+\delta)} > 1$$

then the endemic steady state is the equilibrium state. We can therefore identify the LHS of the two inequalities as being the basic reproduction number, i.e.,

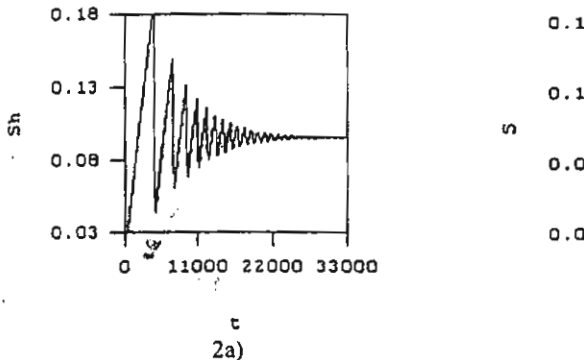
$$R_{0} = \frac{b^{2} \beta_{V} \beta_{h} \mu_{h} N_{T} (B / \mu_{V})}{\mu_{V} (N_{T} + m)^{2} (\mu_{h} + \delta + r) (\mu_{h} + \delta)}$$
(18)

If the susceptible humans are not divided up into juveniles and adults, there is no need for the parameter δ , the rate at which juveniles mature into adults. Setting $\delta = 0$, expression (18) reduces to the expression for the basic reproduction rate obtained in [7]. The modification to R₀ we have introduced to taken into account the presence of an age structure is similar to the one introduced by Esteva and Vargas in [9] where they looked at the changes arising when both a vertical and horizontal mode of transmission of the dengue virus to the mosquitoes are possible.

3.2 Numerical Studies

The main effect of introducing an age structure into the model is change the definition of the basic reproduction rate. Using the values of the parameters similar to those used by Esteva and Vargas ($\mu_h = 0.0000457$, $\mu_V = 0.25$, b = 0.5, $\beta_h = 0.75$, $\beta_V = 1.0$, m = 0.0, r = 0.1428, $N_T = 10,000$, A = 5,000), the value of the basic reproduction number defined in [7] would be 10.5. Numerically solving the set of equations given by Esteva and Vargas (equation (2) in [7]), we obtain the time development of the susceptible human as seen in Figure 2a). In figure 2b), we show the solution to equation (3a), the values of some of the parameters have been changed (i.e., δ = 0.000183, B = 200, μ_h = 0.00003914, μ_V = 0.0714 and r = 0.0714, with the others staying the same). Substituting these values in expression (18), we get $R_0 = 1.8$. In figure 3 and 4, we show the time development of the infected humans and infected mosquitoes for the case of no age structure and an age structure model. In Figure 5, we plot the number of infected humans versus the number of susceptible humans in both a no age structure population and an age structure population. The values of the parameters are such that for both populations, the equilibrium state is the endemic state. The endemic state is a stable spiral state. As we see, the period of fluctuations in the number of individuals in each class is much shorter in the absence of any age structure. The spiraling is much more severe in the absence of the age structure. The age structure appears to calm down the fluctuations.

P. PONGSUMPUN, Y.LENBURY and I.M.TANG



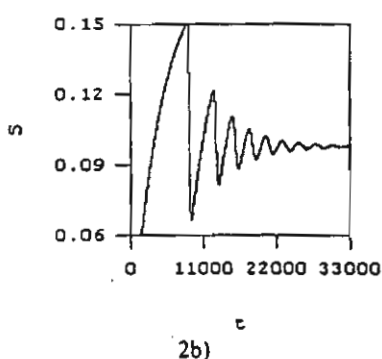
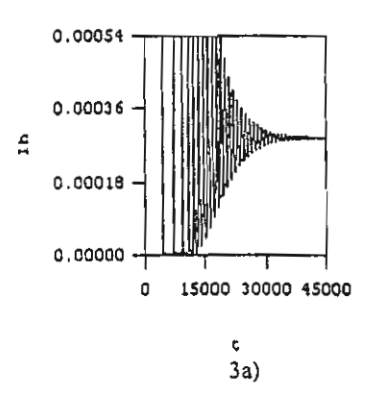


Figure 2. Number of susceptible humans as a function of time. 2a) Solution of equation (2) in [7] for a SIR model of dengue fever transmission with no age structure. 2b) Solution of equation (3a) of the present text for a SIR model having an age structure. The values of the parameters are given in the text.



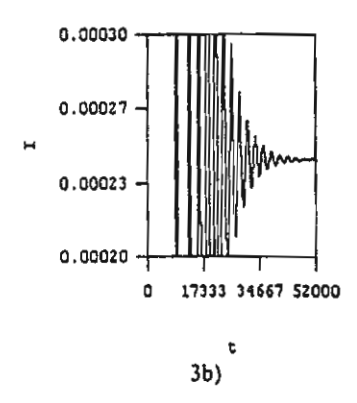
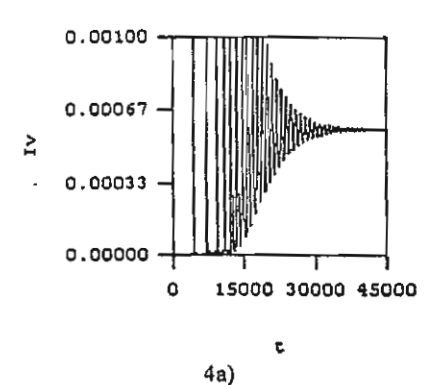
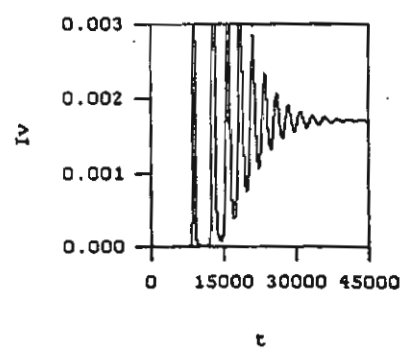


Figure 3. Number of infected humans as a function of time. 3a) Solution of equation (2) in [7] for a SIR model of dengue fever transmission with no age structure. 3b) Solution of equation (3b) of the present text for a SIR model having an age structure. The values of the parameters are given in the text.





4b)

'-55/

Figure 4. Number of infected mosquitoes as a function of time. 4a) Behavior in a non age structure SIR model. 4b) Behavior in an age structured model.

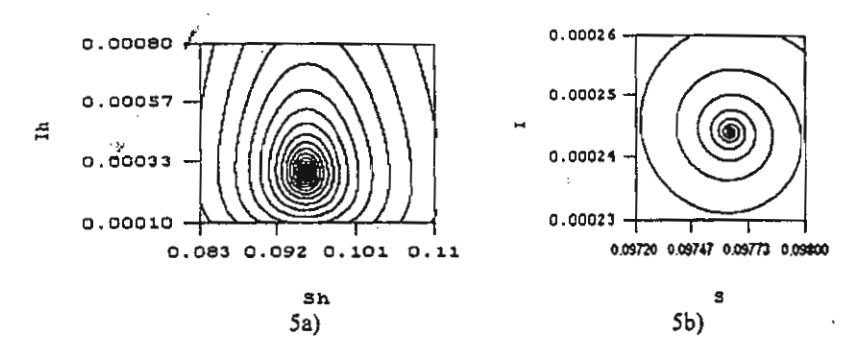


Figure 5. Plot of number of susceptible and infected humans. 5a) Behavior in a non age structured SIR model. 5b) Behavior in an age structured model.

4 Acknowledgements

This work is supported by the Thailand Research Fund with the grant from the Golden Jubilee Ph.D. Program according to the contract number PHD/0154/2543, 3.M.MU/43/B.2.

References

- [1] R. Ross, The prevention of Malaria, 2nd Ed. Murray, London, 1911.
- [2] G. MacDonald, The epidemiology and control of Malaria, Oxford U.Press, London, 1957.
- [3] F.E. McKenzie, Why model Malaria?, Parasitology Today, 16 (2000), 511-516.
- [4] T.P. Monath, Dengue. The risk to developed and developing countries, Proc. Nat. Acad. Sci. USA, 91 (1994), 2395-2400.
- [5] Pan America Health Organization, "Dengue and dengue haemorrhagic fever in the Americas: guidelines for prevention and control", Washington DC: PAHO, 1994.
- [6] J. F. Mendez Galvan, R. M. Castellanos, "Manual para la viglancia epidemiology del dengue", Secretaria de Salud, DF. Mexico, 1994.
- [7] L. Esteva, C. Vargas, Analysis of a dengue disease transmission model, Math. BioSci., 150, (1998), 131-151.
- [8] L. Esteva, C. Vargas, A model for dengue disease with variable human population, J. Math. Bio., 38, (1999), 220-240.
- [9] L. Esteva, C. Vargas, Influence of vertical and mechanical transmission of the dynamics of dengue disease, Math. BioSci., 167,(2000), 51-64.
- [10] M.G. Guzman, G. P. Kouri, J. Bravo, M. Solet, S. Vasquez, M. Santos, R. Villaescusa, P. Basanta, G. Indan, J. M. Ballester., Dengue haemorrhagic fever in Cuba II. Clinical investigations, Trans.R.Soc.Trop.Med.Hyg., 78, (1984), 239-241.
- [11] M. G. Guzman, G.P. Kouri, L. Valdes, J. Bravo, M. Alvarez, S. Vasquez, I. Delgado, S.B. Halstead, *Epidemiologic Studies on Dengue in Santiago de Cuba*, 1997. Am. J. Epidemiol., 152, (2000), 793-799.

P. PONGSUMPUN, Y.LENBURY and I.M.TANG

- [12] Annual Epidemiological Surveillance Report, (1992-1998). Division of Epidemiology, Ministry of Public Health, Royal Thai Government.
- [13] Z. Feng, J. X. Velsco-Hernandez, Competitive exclusion in a vector-host model for the dengue fever, J.Math.Bio., 35, (1997), 523-544.
- [14] C. A. Marques, O. P. Forattini and E. Massad, The basic reproduction number for dengue fever in San Paulo state, Brazil: 1990-1991 Epidemic. Trans. R. Soc. Trop. Med. Hyg., 88, (1994), 58-59.
- [15] J. S. Koopman, D. R. Prevots, M. A. V. Marin, H. G. Dantes, M. L. Z Aquino, I. M. Logini, Jr. and Js. Amor., Determinants and predictors of dengue infection in Mexico, Am. J. Epidemiol., 133 (1991), 1168-1178.
- [16] L.Molineaux and G. Gramiccia, *The Garki Project*, World Health Organization, Gevena, (1980).

Computational Mathematics and Modeling, An International Conference, CMM2002, Bangkok.
Copyright © by East-West J. of Mathematics.
All rights of reproduction in any form reserved.

Transmission of Plasmodium Vivax Malaria

A. Kammanee[†], Y. Lenbury[‡] and I. M. Tang^{*}

†‡ Department of Mathematics, Faculty of Science Mahidol University, Rama 6 Rd. Bangkok 10400, Thailand

* Department of Physics Institute of Science & Technology for Research & Development Salaya Campus, Mahidol University, Nakorn Pathom 71730, Thailand

Abstract

In this paper, we look at the transmission of *Plasmodium vivax* malaria. We divide the host population into 3 categories containing susceptible, infected and dormant population as well as construct the nonlinear differential equations system. By using the basic dynamical method, we obtain the basic reproduction number R_0 , which is considered by the steady state. If $R_0 < 1$, then the malaria becomes extinct; moreover, if $R_0 > 1$ then the equilibrium point is asymptotically stable that endemic state occurs.

1 Introduction

il.

1

Malaria is a serious disease endemic in many parts of Africa, Asia, the Middle East, Central and South America, Hispaniola, and Oceania [10]. There are more than 3 hundred million cases of malaria each year, with between 1 and 1.5 million death mostly among children [7]. Malaria in humans is due to 4 species of the intracrythrocytic protozoa of the genus Plasmodium, i.e., Plasmodium falciparum, Plasmodium vivax, Plasmodium malariae and Plasmodium ovale. Most of the death in childhood is due to P. falciparum. Recently P. vivax has become an enormous problem. In 1997 P. falciparum and P.vivax were found 36.7% and 48.9% of infected population in United states, respectively. In 1997, Luxemburger et al. showed that the transmission rate for P. vivax parasite is higher than that for the P. falciparum.

The mathematical model of malaria has a long history. Ronald Ross was the first person to created a mathematical model of malaria. His model consisted of 4 differential equations, describing changes in the densities of not only the susceptible and the infected host population but also the uninfected (susceptible) and infected mosquitoes [9]. In 2000, McKenzie described the advantages and shortcoming of modeling malaria. He stated that models help us to understand and analyze relationship among variables. Most mathematical model presented so for describe the dynamic for P. falciparum malaria infection [6]. Because of the increased incidence of P. vivax infection, we are faced with the need to model the dynamics of P. vivax infection.

The progression of *P. vivax* malaria differs from *P. falciparum* in that a patient can die from *P. falciparum* but does not die from *P. vivax* infection. Also a person who suffers from *P. falciparum* will recover from the disease (if he does not die from his

illness); a person who is ill with *P. vivax* infected will suffer relapses. The *P. vivax* is induced into blood circulation in the sporozoite form by the bite of an infected female mosquitoes of the genus *Anopheles*. The sporozoite will then migrate to the liver. The sporozoites separate themselves into 2 groups. The first group are the merozoites which invade the blood cell and produce the illness. The second group are the hynozoites which lay dormant in the liver. When the patient is weak, the hynozoites will transform themselves into the merozoites and reinvade the blood cell and reproduce the sickness. These relapses can occur up to five years after the first infection [2]. A mathematical model for *P. vivax* transmission should take this into account.

2 The Mathematical Model

We begin the formulation of the model by dividing the host population (total N_h) into 3 groups; susceptible (S_h') , infected (I_h') and dormant (D_h') population. The dormant population can move to either the infected or susceptible class. The latter occurs since malaria does not confer permanent immunity to further infection. We assume that a susceptible mosquitoes when biting a person in the dormant class will not reinfected the person. We also assume that the number of mosquitoes is constant $(\frac{dN_v}{dt}=0)$. The mosquitos' population (total N_v) is separated into 2 sets; the uninfected (susceptible) (S_v') class and the infected (I_v') class. $N_h = S_h' + I_h' + D_h'$ and $N_v = S_v' + I_v'$ are, respectively, the total human and vector population at time t. The model is assumed that newborns in both population are uninfected.

The time rate of change of any state is equal to the number entering into the state minus the number leaving the state. The dynamic equation describing the density of host population are then

$$\frac{dS_{h}^{'}}{dt} = \lambda N_{h} + (1 - \alpha)r_{1}I_{h}^{'} + r_{3}D_{h}^{'} - (\gamma_{h}^{'}I_{v}^{'} + \mu_{h})S_{h}^{'}$$
 (1)

$$\frac{dI_{h}^{'}}{dt} = \gamma_{h}^{'} I_{v}^{'} S_{h}^{'} + r_{2} D_{h}^{'} - (r_{1} + \mu_{h}) I_{h}^{'}$$
(2)

$$\frac{dD'_{h}}{dt} = \alpha r_{1} I'_{h} - (r_{2} + r_{3} + \mu_{h}) D'_{h}$$
(3)

and
$$\frac{dN_h'}{dt} = (\gamma_h - \mu_h)N_h \tag{4}$$

where all parameter in the model are assumed positive; λ is the natural birth rate of host population; μ_h is the natural mortality rate of human population which will be the same for all classes; r_1^{-1} is the mean life time for the parasite to remain infectious in the human; α is the percentage of individuals leaving the infected state and entering dormant state; r_2 is the relapse rate; r_3 is the recovery rate. The transmission rate for malaria is given by

$$\gamma_h' = b \frac{\beta_h}{N_h + p}$$

where b is the specie-dependent bitting rate of the mosquitoes; p is the population of other animals the the mosquitoes can fed on and β_h is the probability that the P. vivax is passed on by the mosquito to the human. If there is no the dormant state (D_h) and $r_2 = 0$, the model is reduced to the transmission model for P. falciparum.

The rate equations of mosquitoes' population are

$$\frac{dS'_{v}}{dt} = A - \gamma'_{v} I'_{h} S'_{v} - \mu_{v} S'_{v} \tag{5}$$

$$\frac{dI_{v}^{'}}{dt} = \gamma_{v}^{'} I_{h}^{'} S_{v}^{'} - \mu_{v} I_{v}^{'} \tag{6}$$

and
$$\frac{dN_{v}^{'}}{dt} = A - \mu_{v}N_{v} \tag{7}$$

where A is the recruitment rate which is not related to the mosquito's birth rate λ_{v} . The mosquitoes lay eggs which give rise to the larvae stage of the mosquitoes. Only a small number of the larvae will grow into the adult stage. This number depend on the carrying capacity of the environment and not on the number of eggs laid at [2].

We assume that the total number of humans and mosquitoes are constant, $N_h = S_h' + I_h' + D_h'$ and $N_h = S_v' + I_v'$. We now introduce the normalized variables $S_h = \frac{S_h'}{N_h}$, $I_h = \frac{I_h'}{N_h}$, $D_h = \frac{D_h'}{N_h}$, $S_v = \frac{S_v'}{N_v}$ and $I_v = \frac{I_v'}{Nv}$. The domain of acceptable solution is given by

$$\Omega = \{ (S_h, I_h, D_h, S_v, I_v) | 0 \le S_h, I_h, D_h, S_v, I_v \le 1 \}$$

The dynamic equations can now be rewritten as

띩

$$\frac{dS_h}{dt} = \lambda + (1 - \lambda)r_1I_h + r_3D_h - (\gamma_hI_v + \mu_h)S_h$$
 (8)

$$\frac{dI_h}{dt} = \gamma_h I_v S_h + r_2 D_h - (r_1 + \mu_h) I_h \tag{9}$$

$$\frac{dD_h}{dt} = \alpha r_1 I_h - (r_2 + r_3 + \mu_h) D_h \tag{10}$$

$$\frac{dS_v}{dt} = \mu_v - \gamma_v I_h S_v - \mu_v S_v \tag{11}$$

and
$$\frac{dI_{v}}{dt} = \gamma_{v}I_{h}S_{v} - \mu_{v}I_{v}$$
 (12)

where $\gamma_h = \gamma_h' \frac{\mu_h}{A}$ and $\gamma_v = \gamma_v' N_h$. We use $S_h + I_h + D_h = 1$ and $S_v + I_v = 1$ to reduce the number of differential equations from 5 to 3 since $\frac{dS_h}{dt} = -(\frac{dI_h}{dt} + \frac{dD_h}{dt})$

and
$$\frac{dS_v}{dt} = -\frac{dI_v}{dt}$$
. We thus have

$$\frac{dI_h}{dt} = \gamma_h I_v (1 - I_h - D_h) + r_2 D_h - (r_1 + \mu_h) I_h \tag{13}$$

$$\frac{dD_h}{dt} = \alpha r_1 I_h - (r_2 + r_3 + \mu_h) D_h \tag{14}$$

and
$$\frac{dI_v}{dt} = \gamma_v I_h (1 - I_v) - \mu_v I_v \tag{15}$$

2.1 Equilibrium State

Setting the RHS of (13)-(14) to zero and solving for the 3 variables, we gain two equilibrium states; the disease free state $E_0=(0,0,0)$ and the endemic state $E_1=(I_h^*,D_h^*,I_v^*)$ where $D_h^*=\frac{\alpha r_1}{r_1+r_3+\mu_h}I_h^*$; $I_v^*=\frac{\gamma_v}{\gamma_vI_h^*+\mu_v}I_h^*$ and $I_h^*=\frac{R_0-1}{R_0M}$ with $M=1+\frac{r_1+\mu_h}{\gamma_h}+\frac{\alpha r_1(\gamma_h-r_2)}{\gamma_h(r_2+r_3+\mu_h)}$ and the basic reproduction number is found to be given by

$$R_0 = \frac{\gamma_h \gamma_v}{\mu_v (r_1 + \mu_h - \frac{\alpha r_1 r_2}{r_2 + r_3 + \mu_h})}$$
(16)

Examiniting the expressing above, we find that physical values of I_h^* , D_h^* and I_v^* are possible when $R_0 > 1$. When $R_0 < 1$, the epidemic state is not possible. This leaves the disease free state as the only possibility.

2.2 Locally Asymptotical Stability

The local stability of the equilibrium state is determined by the Jacobian (gradient) matrix evaluated at the equilibrim states. We find its eignvalues by solving the determinant equation det $|J - \lambda I| = 0$ where

$$J(I_h^*, D_h^*, I_v^*) = \begin{pmatrix} -(r_1 + \mu_h + \gamma_h I_h^*) & r_2 - \gamma_h I_v^* & \gamma_h (1 - I_h^* - D_h^*) \\ \alpha r_1 & -(r_2 + r_3 + \mu_h) & 0 \\ \gamma_v (1 - I_v^*) & 0 & -(\gamma_v I_h^* - \mu_v) \end{pmatrix}$$

The equilibrium state is stable if the real parts of all the eigenvalus are negative. The trajectory of the state towards this equilibrium occurs when two of the eigenvalues are complex conjugates pairs.

2.2.1 Disease Free State

The system equation (4), the gradient matrix at disease free state, E_0 , is given by

$$J(0,0,0) = \begin{pmatrix} -(r_1 + \mu_h) & r_2 & \gamma_h \\ \alpha r_1 & -(r_2 + r_3 + \mu_h) & 0 \\ \gamma_v & 0 & -\mu_v \end{pmatrix}$$

The charectesistic equation is found that is $\lambda^3 + a_1\lambda^2 + a_2\lambda + a_3 = 0$ where

$$a_1 = r_1 + r_2 + r_3 + 2\mu_h + \mu_v$$

$$a_2 = (r_1 + \mu_h)(r_2 + r_3 + \mu_h + \mu_v) + \mu_v(r_2 + r_3 + \mu_h) - \gamma_h\gamma_v - \alpha r_1 r_2$$

$$a_3 = \mu_v(r_1 + \mu_h)(r_2 + r_3 + \mu_h) - \gamma_h\gamma_v(r_2 + r_3 + \mu_h) - \alpha r_1 r_2 \mu_v$$

The real parts of eigenvalues will be negative if $a_1 > 0$. Two of the eigenvalues will be conjugate pairs if $a_3 > 0$. We see that this condition is satisfied if $R_0 < 1$.

2.2.2 Endemic Disease State

The characteristic equation for the gradient matrix evaluated at the endemic disease state is given by

$$\lambda^3 + a_1 \lambda^2 + a_2 \lambda + a_3 = 0 \tag{17}$$

where

1

$$a_{1} = r_{1} + r_{2} + r_{3} + 2\mu_{h} + \mu_{v} + (\gamma_{h} + \gamma_{v})I_{h}'$$

$$a_{2} = (r_{1} + \mu_{h} + \gamma_{h}I_{h}')(r_{2} + r_{3} + \mu_{h}) + \gamma_{v}I_{h}' + \mu_{v}) + (r_{2} + r_{3} + \mu_{h})(\gamma_{v}I_{h}' + \mu_{v})$$

$$- \gamma_{v}\gamma_{h}(1 - I_{v}')(1 - I_{h}' - D_{h}') - \alpha r_{1}(r_{2} + \gamma_{h}I_{v}')$$

$$a_{3} = -det(J)$$

The root of equation (17) will have a negative real part when $a_1 > 0$. We find that this is always true if $R_0 > 1$. We have a stable spiral mode if $a_2 > 0$. When $a_2 < 0$, but $a_1 > 0$, the trajectory will be a stable star mode.

3 Discussion

3.1 The Basic Reproduction Number

The basic reproduction number R_0 , is defined as the number of secondary infections produced by an initial infect [7]. MacDonald [5] defined R_0 for P. falciparum malaria to be

$$R_0 = \frac{ma^2b_1b_2e^{-\mu T}}{\mu r} \tag{18}$$

where m is the ratio of mosquito to post population density; b_1 is the transmission of the infectiousness from an infected human to a mosquito; b_2 is the transmission of the infectiousness from an infected mosquito to a human; μ is the daily death of the mosquito; T is the parasite's developmental period in the mosquito; r is the recovery rate in human and $e^{-\mu T}$ is the probability that the mosquito survives the developmental period of the parasite from the initial infection to become infectious.

MacDonald concluded that changes in the mosquito death would have most effect on R_0 . Here we are interested in the effects of the relapse on the transmission of P.vavix malaria. We find that R_0 increase as the relapse rate increase.

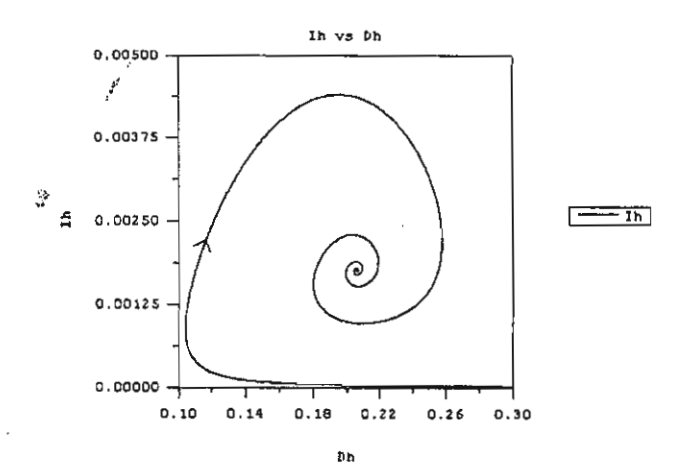


Fig 5. Initial behaviour of the proportions I_h and D_h . The parameters are the same as in Figure 3. There is a threshold parameter R_0 and the disease can exist in the epidemic state if and only if R_0 exceeds one. The disease-free equilibrium exists and is globally stable if $R_0 \leq 1$. The endemic equilibrium is a stable spiral state.

References

- [1] L. Esteva and C. Vargas, Analysis of Dengue Disease Transmission Model, Math BioSci, 150(1998) 131-161.
- [2] A. Kammanee, N. Kanyamee, I.M. Tang. Basic Reproduction Number for Transmission of Plasmodium Vivax Malaria, Southeast Asian J. Trop. Med. Public Health, 32(2001) 702-706.
- [3] C. Luxemburger, F. Ricci, F. Noten, D. Raimond and S. Bather, *The Epidemiology of Severe Malaria in an Area of Low Transmission in Thailand*, Transactions of The Royal Society of Tropical Medicine and Hygiene, **19**(1997) 105-111.
- [4] G. MacDonald, "The Epidemiology and Control of Malaria". Oxford Uni. Press, 1957.
- [5] D. P. Mason and F.E. Mckenzie, Blood-Stage Dynamics and clinical Implications of Mixed Plasmodium Vivax-Plasmodium Falciparum infections, The American Society of Tropical Medicine and Hygene, 603 (1999) 367-374.
- [6] F. E. McKenzie, Why Model Malaria?, Parasitology Today, 16(2000), 511-516.
- [7] G. A. Ngwa and W.S. Shu, A Mathematical Model for Endemic Malaria with Variable Human and Mosquito Populations, Mathematical and Computer Modelling, 32 (2000) 747-763.
- [8] R. Ross, "The Prevention of Malaria", 2nd ed., Murray, London, 1991.
- [9] R. M. Anderson and R. M. May, "Infectious Diseases of Humans: Dynamics and Control", Oxford Uni. Press, 1992.
- [10] http://www.cdc.gov/mmwr/preview/mmwrhtml/ss5005a1.htm

Computational Mathematics and modeling, An International Conference, CMM2002, Bangkok Copyright©by East-West J. of Mathematics.

All rights of reproduction in any form reserved.

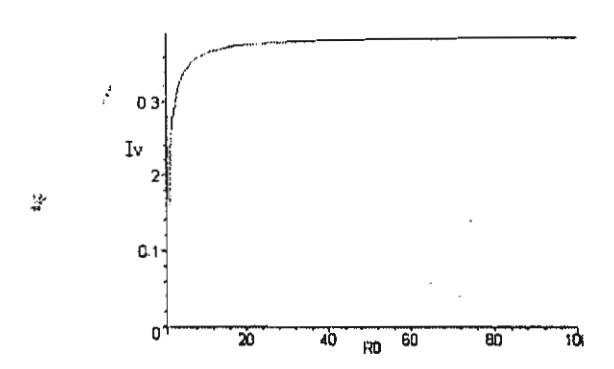


Fig 1. Diagram showing graph of R_0 against I_v where $\mu_h = \frac{1}{365 \times 60}$; $r_1 = 0.76$; $r_2 = 0.5$; $r_3 = 0.001$; $\alpha = 0.84$; $\mu_v = 0.25$; $\gamma_h = 0.1428$; $\gamma_v = 0.5$

We plotted R_0 again I_v^* . In figure 1,we can clearly see that the proportions of infected mosquitoes vary with the basic reproduction number. When R_0 is below 50, a small change in R_0 will lead to a large changes in I_v^* . However for high R_0 , the increase is at a slower rate. Reducing the density of the mosquitos' population will not have a significant effect in the endemic regions where the basic reproduction number is large (R_0 decline as the density of the mosquito decline)

3.2 Simulation

We have numerically solved equations (8) - (12) using a computer. The program was run for different sets of initial conditions. The steady state solutions are the same. We have formed the endemic steady state solution to be unique and globally and asymptotically stable. We have pick set of the values of the variable appearing in the expressions for the equilibrium states to be $I_h = 0.5$, $D_h = 0.25$ and $I_v = 0.00001$. For case of $R_0 > 1$, we formed that the endemic equilibrium would be locally and asymptotically stable. Numerical simulation confirmed this result.

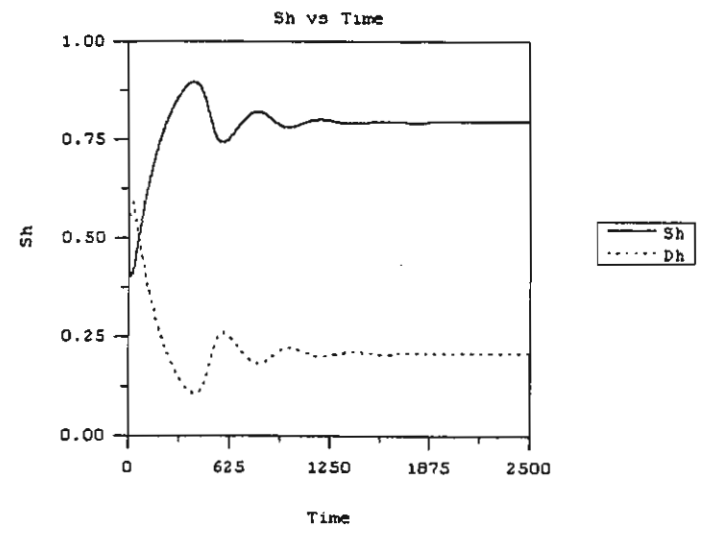


Fig 2. Initial behavior of the proportions S_v and D_v with time (days). The parameters are $r_2 = 0.000007$; $\alpha = 0.65$; $r_3 = 0.005$; $r_1 := 0.91$; $\mu_v := 0.25$; $\gamma_h := 1.95$; and $\gamma_v := 0.25$;

A. KAMMANEE, Y. LENBURY AND I. M. TANG

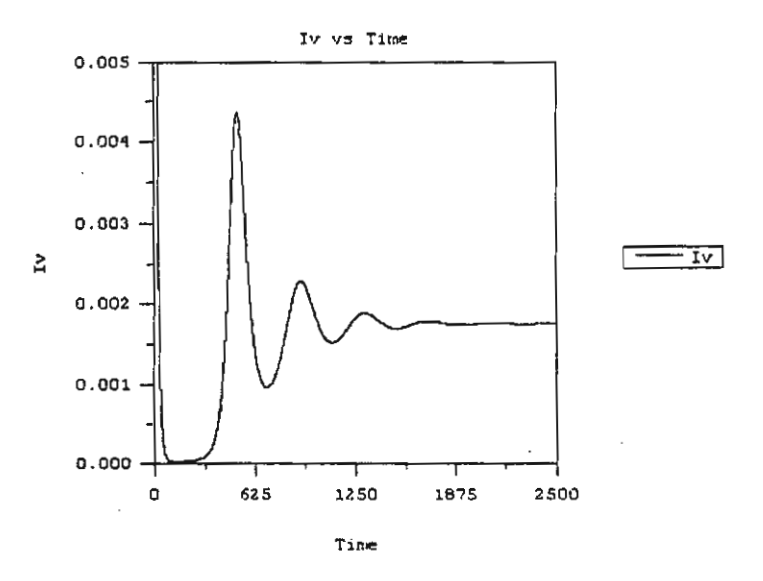


Fig 3. Initial behaviour of the proportions I_v with time (days). The parameters are the same as Figure 2

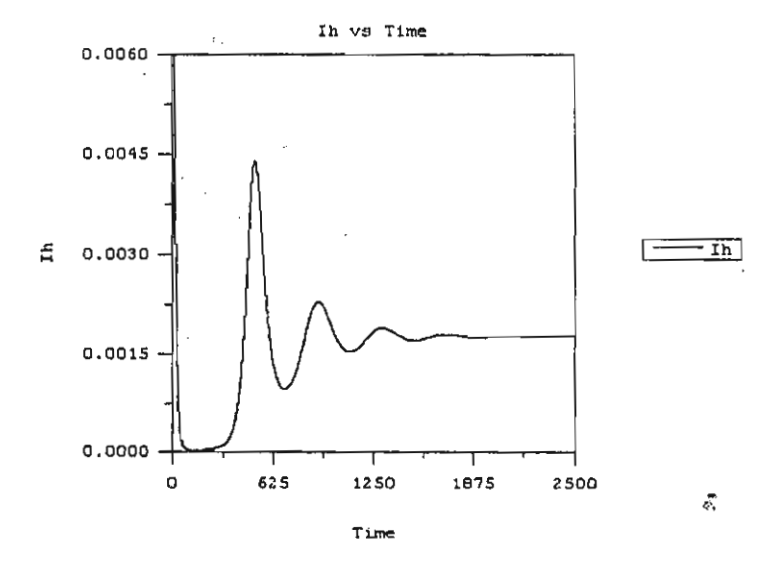


Fig 4. Initial behaviour of the proportions I_h with time (days). The parameters are the same as in Figure 2

THE EFFECT OF MIGRANT WORKERS ON THE TRANSMISSION OF MALARIA

N. Kanyamee[†], Y. Lenbury[‡] and I. M. Tang^{*}

†‡ Department of Mathematics and * Department of Physics
Faculty of Science, Mahidol University, Rama 6 Rd. Bangkok 10400, Thailand
*Institute of Science & Technology for Research & Development
Salaya Campus, Mahidol University, Nakorn Pathom 71730. Thailand

Abstract

In this research, we model the transmission of malaria in the movement of population by considering a system of nonlinear differential equations in the Susceptible-Infected-Susceptible (SIS) model. The human population is divided into a host population (in community) class and a migrant workers class. We analyze the behavior of our system. The conditions for equilibrium are obtained by looking at the conditions for zeros in a third degree polynomial. By considering the standard dynamical method, the percentage of infectious migrant worker is used as an adjustable parameter. Numerical simulations are used to illustrate the results for supporting our theoretical data.

1 Introduction

Malaria is a serious acute and chronic relapsing infection to human [14]. It is transmitted to human by biting of mosquitoes in genus Anopheles. Four types of protozoa species (strain) belonging to the genus Plasmodium, namely P. falciparum, P. vivax, P.malariae and P. ovale, cause an infection. The World Health Organization estimated that there are over one million child deaths per year in sub-Saharan Africa, 300-500 million cases of malaria per year and more than two billion people are at risk throughout the world [13].

The first person who attempts to construct a mathematical model of the dynamics of malaria transmission was Ronald Ross[9]. His model consisted of a few differential equations to describe changes in the densities of susceptible and infected people and mosquitoes. He found that for any given set of malariological circumstances some minimum number of mosquitoes, above zero, was needed to keep transmission going. If number fell below, the disease becomes extinct. After Ross demonstrated that malaria are transmitted by mosquitoes, he stated [8] that To say that a disease depends upon certain factors is not to say much, until we can also form an estimate as to how largely each factor influences the whole result. Recently, McKenzie[8] had pointed out that models can be powerful tools for integrating information from different disciplines. In 1950, Macdonald [6], extended the model by introduced a layer

of biological realism (infection rate) to the model. He studies the influences of the mosquito malaria-infection rate. The Ross-Macdonald model is used to analyze equilibrium state for malaria in term of the influence of the mosquito malaria-infection rate on the human infection rate and of the human infection rate on the mosquito infection rate. Other advance models about malaria transmission have been introduced. In 2000, A. Kammanee, N. Kanyamee and I.M. Tang[3] have introduced a new model for the transmission of *P.vivax* malaria. The population is divided into 4 classes by considering the possibility of relapse. In the present work, we use some parameter and introduce a migration factor from this model.

The incidences of malaria have increased in many regions in the world and in area which people thought was disease free [7]. One of the important factor that leads to the malaria transmission is the movement of migrant worker due to the poverty. The spread of disease is enhanced when population move from that place to the others. In Luxemburger[5] study, a town located on the western border of Thailand, reported that in the area adjacent to Burma there are significant population movements. This movement was thought to be a major factor in the regional spread of multi-drug resistance. There are many evidences in other regions in the world supporting this idea [13]. At the beginning of the 1960's malaria had been eradicated from Tajikistan, but it reappeared an endemic in the 1990's in the area bordering Afghanistan. Laboratoryconfirmed malaria cases increased from 175 in 1990 to 2400 in 1994, mainly from the southern border areas. The appearance of malaria in the United Kingdom was due to the infection being brought in from abroad. Of the 1,887 malaria cases in the United Kingdom, 704 occurred in people who, while living in the UK, traveled to visit family in their country of origin. In Cambodia, about 2.5 million people have malaria. 26% of the population is considered to live in areas at risk of malaria transmission. The most intense transmission occurs in the forested areas along the Thai border and in the northeastern part of the country. In this study we are interested in the effect of migration in the malaria transmission. The identification and understanding of the influence of those population movements can improve the prevention measures and malaria control programs.

2 The Mathematical Model

In our study, we construct a simple model for malaria transmission. We assume that the human population and mosquito population (N_V) are constants; resulting birth and death rates are the same. The total population is divided into two populations, a host population (N_T) with a total population of a migrant worker population (N_W) . The host population is divided into two subclasses, susceptible (S') and infected (I') host population. The migrant population is also divided into two subclasses that are susceptible (S'_w) and infected (I'_w) worker population. In the standard transmission model for P. vivax [3], the model has 4 subclasses with no migration term. We consider the effect of migrant workers by adding the migration term into the model. The mosquito (vector) population is also divided into two subclasses, uninfected (susceptible) (S'_v) and infected (I'_v) mosquito population. Since malaria does not give a

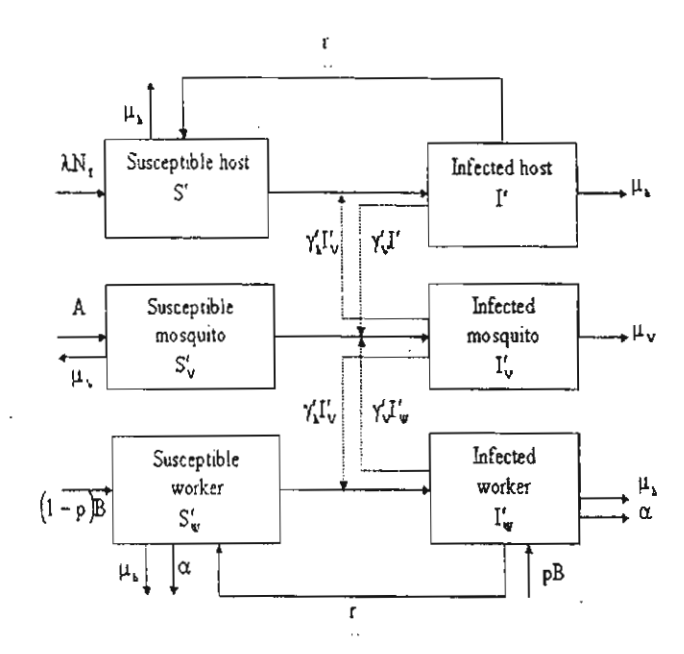
•

3

ŝ

permanent immunity to further infection, we allow the individual in an infected class to reenter into the susceptible class, with rate r, the rate at which they loss their immunity.

The flowchart of the disease is shown in the figure below. We assume that the workers migrate in and out at constant rates. The infectious migrant workers enter the country with percentage p. The time rate of change of any class is equal to the number entering into the class minus the number leaving the class. The migrant worker population moves out rom country with rate α , the reciprocal of the time migrant workers stay in the country. A is the recruitment rate of mosquitoes. B is the recruitment rate of migrant workers. λ is the birth rate among host population. We assume that the migrant worker population stays long enough to reproduce. μ_h is the natural death rate of human and μ_v is the natural death rate of moquitoes.



The dynamic equations for this SIS model with migration is described by the flowchart are

$$\frac{dS'}{dt} = \lambda N_T + rI' - \gamma'_h I'_v S' - \mu_h S' \tag{1}$$

$$\frac{dI'}{dt} = \gamma_h' I_v' S' - (\mu_h + r) I' \tag{2}$$

$$\frac{dS'_{w}}{dt} = (1-p)B + rI'_{w} - \gamma'_{h}I'_{v}S_{w}' - (\mu_{h} + \alpha)S_{w}'$$
(3)

and
$$\frac{dI_{w'}}{dt} = pB + \gamma'_{h}I'_{v}S_{w'} - (\mu_{h} + \alpha + r)I'_{w}$$
 (4)

For vector (mosquito) transmitted disease, $\gamma_h^{'}$ is the unrenormalized rate of trans-

mission of malaria parasite from mosquitoes to humans as shown by Esteva and Vargas [2] and [3]

$$\gamma_h' = \frac{b\beta_h}{N_T + N_m + m} \tag{5}$$

where species-dependent biting rate b of mosquitoes is the average number of bites per mosquito per day; m denote the number of other animals available as blood sources and β_h is the transmission probability that parasite passed from vector to human and continue to thrive in the human.

The time rates of changes of the mosquito population are given by

$$\frac{dS'_{v}}{dt} = A - \gamma'_{v}I'S'_{v} - \gamma'_{v}I'_{w}S'_{v} - \mu_{v}S'_{v}$$
 (6)

and
$$\frac{dI'_{v}}{dt} = \gamma'_{v}I'S'_{v} + \gamma'_{v}I'_{w}S'_{v} - \mu_{v}I'_{v}$$
 (7)

where γ_{v} is the unrenormalized rate at which the mosquito becomes infected with the malaria parasites once the mosquito has bitten an infected human and it is given[2]

$$\gamma_{v}^{'} = \frac{b\beta_{v}}{N_{v} + m} \tag{8}$$

where β_v is the transmission probability that parasite passed on an infection from human to vectors.

When the total population of each group is constant, we normalized the variables

by dividing by
$$N_T$$
, N_w or N_v ($N_w = \frac{B}{\mu_h + \alpha}$, $N_v = \frac{A}{\mu_v}$), i.e., the proportions $S = \frac{S'}{N_T}$, $I = \frac{I'}{N_T}$, $S_w = \frac{S'_w}{B/(\mu_h + \alpha)}$, $I_w = \frac{I'_w}{B/(\mu_h + \alpha)}$, $S_v = \frac{S'_v}{A/\mu_v}$. $I_v = \frac{I'_v}{A/\mu_v}$. Since we have $S + I = 1$, $S_w + I_w = 1$, and $S_v + I_v = 1$, only three of the six

variables will be independent. Picking the three to be I, I_w , and I_v , we have

$$\frac{dI}{dt} = \gamma_h I_v(1 - I) - (\mu_h + r)I \tag{9}$$

$$\frac{dI_w}{dt} = p(\mu_h + \alpha) + \gamma_h I_v (1 - I_w) - (\mu_h + \alpha + r) I_w \tag{10}$$

and
$$\frac{dI_v}{dt} = \gamma_v I(1 - I_v) + \gamma_v (\frac{N_w}{N_T}) I_w (1 - I_v) - \mu_v I_v$$
 (11)

The domain region Λ of biological interest is given by

$$\Lambda = \{(S, I, S_w, I_w, S_v, I_v) | 0 \le S, I, S_w, I_w, S_v, I_v \le 1, 0 \le S + I \le 1,$$

$$0 \le S_w + I_w \le 1, 0 \le S_v + I_v \le 1 \}. \tag{12}$$

This domain is positively invariant under the flow induced by the six equations, as the vector field on the boundary does not point to the exterior.

301

2.1 Equilibrium points of the model

We use the standard dynamical modelling methods to analyze our model. The equilibrium points of our system are obtained by setting the RHS of equations (9) to (11) to zero. The equilibrium points are given by:

$$I = \frac{\gamma_h I_v}{\gamma_h I_v + \mu_h + r} \tag{13}$$

$$I_{w} = \frac{p(\mu_{h} + \alpha) + \gamma_{h}I_{v}}{\gamma_{h}I_{v} + \mu_{h} + \alpha + r}$$

$$\tag{14}$$

and
$$I_{v} = \frac{\gamma_{v}I + \gamma_{v}(\frac{N_{w}}{N_{T}})I_{w}}{\gamma_{v}I + \gamma_{v}(\frac{N_{w}}{N_{T}})I_{w} + \mu_{v}}$$
(15)

Substituting Eq.(13) and (14) into Eq. (15), Eq. (15) can be rearranged as a cubic equation in I_{ν} , i.e.,

$$b_1 I_v^3 + b_2 I_v^2 + b_3 I_v + b_4 = 0 (16)$$

where

1

$$b_{1} = \gamma_{h}^{2} \gamma_{v} + \gamma_{h}^{2} \gamma_{v} \left(\frac{N_{w}}{N_{T}}\right) + \gamma_{h}^{2} \mu_{v}$$

$$b_{2} = \gamma_{h} \gamma_{v} (\mu_{h} + \alpha + r) + \gamma_{h} \gamma_{v} \left(\frac{N_{w}}{N_{T}}\right) p(\mu_{h} + \alpha) + \gamma_{h} \gamma_{v} \left(\frac{N_{w}}{N_{T}}\right) (\mu_{h} + r)$$

$$+ \gamma_{h} \mu_{v} (\mu_{h} + \alpha + r) + \gamma_{h} \mu_{v} (\mu_{h} + r) - \gamma_{h}^{2} \gamma_{v} - \gamma_{h}^{2} \gamma_{v} \left(\frac{N_{w}}{N_{T}}\right)$$

$$b_{3} = \gamma_{v} \left(\frac{N_{w}}{N_{T}}\right) p(\mu_{h} + \alpha) (\mu_{h} + r) + \mu_{v} (\mu_{h} + r) (\mu_{h} + \alpha + r)$$

$$- \gamma_{h} \gamma_{v} (\mu_{h} + \alpha + r) - \gamma_{h} \gamma_{v} \left(\frac{N_{w}}{N_{T}}\right) p(\mu_{h} + \alpha) - \gamma_{h} \gamma_{v} \left(\frac{N_{w}}{N_{T}}\right) (\mu_{h} + r)$$
and
$$b_{4} = -\gamma_{v} \left(\frac{N_{w}}{N_{T}}\right) p(\mu_{h} + \alpha) (\mu_{h} + r)$$

$$(17)$$

Denoting I_v^* as the solutions of Eq. (16), we have a nonzero equilibrium state exists if at least one solution of Eq. (16) is real and positive. This will happen when either

(i)
$$b_{2} < 0, b_{3} > 0$$
 $b_{2}^{2} > 3b_{1}b_{3}, and \Omega < 0$
or (ii) $b_{2} \ge 0, b_{3} < 0$ and $\Omega < 0$
or (iii) $b_{2} > 0, b_{3} \ge 0, b_{2}^{2} > 3b_{1}b_{3}, and \Omega < 0$
or (iv) $(\frac{1}{54b_{1}^{3}}(9b_{1}b_{2}b_{3} - 27b_{1}^{2}b_{4} - 2b_{2}^{3}) + (\frac{\Omega}{4})^{\frac{1}{2}})^{\frac{1}{3}}$
 $+ (\frac{1}{54b_{3}^{3}}(9b_{1}b_{2}b_{3} - 27b_{1}^{2}b_{4} - 2b_{2}^{3}) - (\frac{\Omega}{4})^{\frac{1}{2}})^{\frac{1}{3}} > \frac{b_{2}}{3b_{1}}, and \Omega > 0$ (18)

where

$$\Omega = \frac{4}{27}b_1b_3^3 - \frac{1}{27}b_2^2b_3^2 + \frac{4}{27}b_2^3b_4 - \frac{2}{3}b_1b_2b_3b_4 + b_1^2b_4^2.$$

Proof of these conditions is given in the appendix.

If any of the above conditions are met, then one of the solutions of Eq. (16) will $\cdot \cdot$ be real and positive. Calling this solution I_v^* , the equilibrium state will be

$$E = (S^*, I^*, S_w^*, I_w^*, S_v^*, I_v^*)$$

where I_v^* is the solution of Eq.(16),

$$I^* = \frac{\gamma_h I_v^*}{\gamma_h I_v^* + \mu_h + r}, I_w^* = \frac{p(\mu_h + \alpha) + \gamma_h I_v^*}{\gamma_h I_v^* + \mu_h + \alpha + r}.$$
 (19)

 $S^* = 1 - I^*$, $S_w^* = 1 - I_w^*$, and $S_v^* = 1 - I_v^*$ (Once it has been established that a positive real solutions of Eq.(16) exists, numerical method can be used to find it).

2.2 Stability of the equilibria

The local stability of the equilibrium points can be determined by linearizing the system (Eq.(9) to (11)) about the equilibrium point (I^*, I_w^*, I_v^*) . The eigenvalues are found by diagonalizing the Jacobian matrix or det $|J - \lambda I| = 0$. This gives the Jacobian matrix

$$J(I^*, I_w^*, I_v^*) = \begin{pmatrix} \gamma_h I_v^* - (\mu_h + r) & 0 & \gamma_h (1 - I^*) \\ 0 & -\gamma_h I_v^* - (\mu_h + \alpha + r) & \gamma_h (1 - I_w^*) \\ \gamma_v (1 - I_v^*) & \gamma_v (\frac{N_w}{N_T}) (1 - I_v^*) & -\gamma_v I^* - \gamma_v (\frac{N_w}{N_T}) I_w^* - \mu_v \end{pmatrix}$$

Computing this matrix and noting

$$\gamma_{h}I_{v}^{*} + (\mu_{h} + r) = \frac{\gamma_{h}I_{v}^{*}}{I^{*}}$$

$$\gamma_{h}I_{v}^{*} + (\mu_{h} + \alpha + r) = \frac{p(\mu_{h} + \alpha) + \gamma_{h}I_{v}^{*}}{I_{w}^{*}}$$
and
$$\gamma_{v}I^{*} + \gamma_{v}(\frac{N_{w}}{N_{T}})I_{w}^{*} + \mu_{v} = \frac{\gamma_{v}I^{*} + \gamma_{v}(\frac{N_{w}}{N_{T}})I_{w}^{*}}{I_{v}^{*}}, \tag{20}$$

303

we get the following characteristic equation

$$\lambda^3 + c_1 \lambda^2 + c_2 \lambda + c_3 = 0 \tag{21}$$

where

$$c_{1} = \frac{\gamma_{h}I_{v}^{*}}{I^{*}} + (\frac{p(\mu_{h} + \alpha) + \gamma_{h}I_{v}^{*}}{I_{w}^{*}}) + (\frac{\gamma_{v}I^{*} + \gamma_{v}\frac{N_{w}}{N_{T}}I_{w}^{*}}{I_{v}^{*}})$$

$$c_{2} = (\frac{p(\mu_{h} + \alpha) + \gamma_{h}I_{v}^{*}}{I_{w}^{*}})(\frac{\gamma_{v}I^{*} + \gamma_{v}\frac{N_{w}}{N_{T}}I_{w}^{*}}{I_{v}^{*}}) - \gamma_{h}\gamma_{v}(1 - I_{v}^{*})((1 - I^{*}) + \frac{N_{w}}{N_{T}}(1 - I_{w}^{*}))$$

$$- \frac{\gamma_{h}I_{v}^{*}}{I^{*}}(\frac{p(\mu_{h} + \alpha) + \gamma_{h}I_{v}^{*}}{I_{w}^{*}}) + \frac{\gamma_{v}I^{*} + \gamma_{v}\frac{N_{w}}{N_{T}}I_{w}^{*}}{I_{v}^{*}})$$

$$and * c_{3} = \frac{\gamma_{h}}{I^{*}}(\frac{p(\mu_{h} + \alpha) + \gamma_{h}I_{v}^{*}}{I_{w}^{*}})(\gamma_{v}I^{*} + \gamma_{v}\frac{N_{w}}{N_{T}}I_{w}^{*})$$

$$- \gamma_{h}\gamma_{v}(1 - I_{v}^{*})(\frac{\gamma_{h}I_{v}^{*}}{I^{*}}\frac{N_{w}}{N_{w}}(1 - I_{w}^{*}) + (1 - I^{*})(\frac{p(\mu_{h} + \alpha) + \gamma_{h}I_{v}^{*}}{I^{*}})). \tag{22}$$

The eigenvalues are the solutions of (21) will be negative real part when the coefficient c_1, c_2 , and c_3 satisfy the Routh-Hurwith criteria[1], i.e.

$$c_1 > 0 \tag{23}$$

$$c_3 > 0 \tag{24}$$

$$and \quad c_1c_2 > c_3 \tag{25}$$

We see that the first condition is always satisfied hence we only need to consider conditions (24) and (25) to establish whether the equilibrium point is locally and asymptotically stable.

3 Discussion

In this section, we performed some numerical simulations to illustrate the results of our model. The numerical values of the parameters were picked so that conditions (23) to (25) and (18) are satisfied. The numerical program was written in Fortran to solve the set of Eq. (9)to (11). Using the parametric values in unit of year, $\gamma_h = 0.27$, $\gamma_v = 0.7$, $\mu_h = 1/60$, $\mu_v = 15.0$, r = 0.16, $\alpha = 0.2$, $N_T = 100,000$, $N_w = 50,000$, and $N_v = 2,000,000$. At time t = 0, the following initial conditions were used as I(0) = 0.45, $I_w(0) = 0.6$, and $I_v(0) = 0.5$ where the other variables are obtained from S = 1 - I, $S_w = 1 - I_w$, and $S_v = 1 - I_v$.

The general behavior of the model is shown in figures 1 to 5 where the numerical results are plotted in time (year) versus the normalized populations. Figures 1 to 4 show the initial and long time behavior of human populations plotted on the same graph

when p increases from 0.00005 to 0.5 and 0.95 respectively. The equilibrium point is given by $E = (S^*, I^*, S_w^*, I_w^*, S_v^*, I_v^*)$ are (0.999999, 0.00000125, 0.999971, 0.00002929. 0.999999, 7.35882×10^{-7}), (0.989033, 0.0109673, 0.708703, 0.291297, 0.992744, 0.0072557), and (0.979614, 0.0203857, 0.550844, 0.986384, 0.0136164) when p increases from 0.00005 to 0.5 and 0.95 respectively. In Figure 1, we see that when infected workers first introduced into the community for small values of p the susceptible worker population is rapidly rising to 0.999971 and infected worker population is declining to 0.708703. In Figure 2 where p is set to be 0.5, the susceptible worker population keep on increasing but at a rate smaller than previously. When p is 0.95, we see in Figure 3 that the normalized infected worker population is higher than the normalized susceptible worker population whereas the normalized host population has the same behavior with a smaller change. Figure 4 represents the long-term behavior of the normalized human population. At first, they change but as time changed they become stable for a long time period (year). Figure 5 represents the behavior of the normalized mosquito population. It appears not to change as we increase p but it actually does. In conclusion, the higher percentage of infected workers affects high level of infected population and small level of susceptible population.

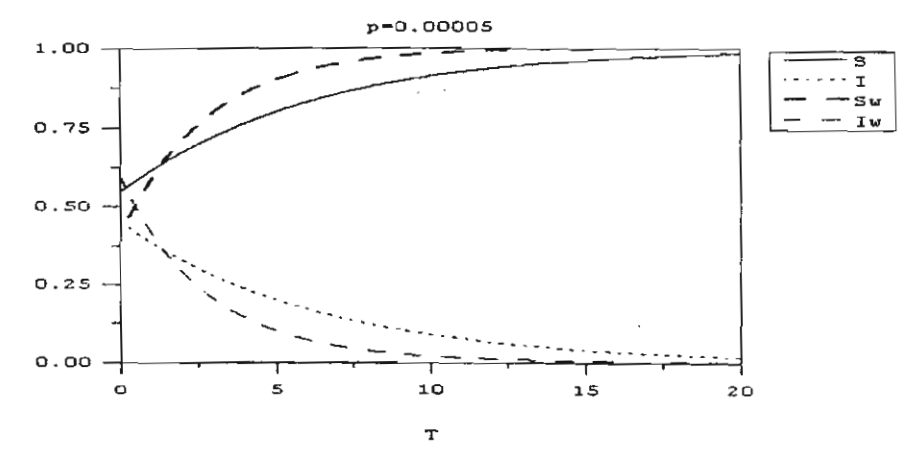


Fig 1. Initial behaviour of the human proportions S, I, S_w and I_w with time (years) when p is 0.00005.

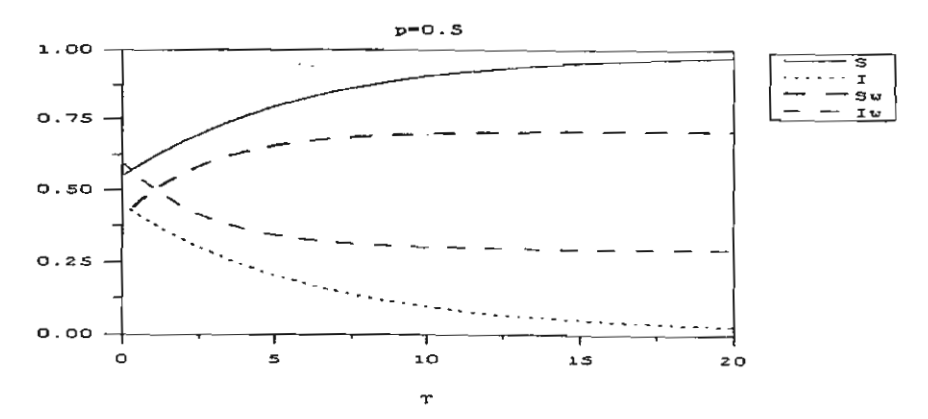


Fig 2. Initial behaviour of the human proportions S, I, S_w and I_w with time (years) when p is 0.5.

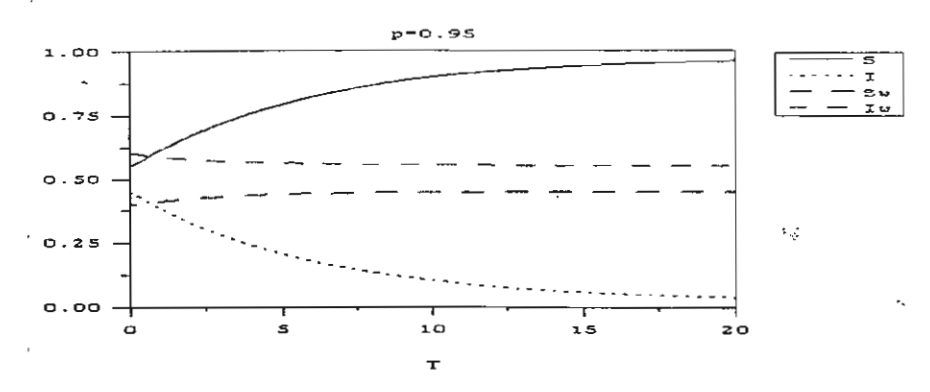


Fig 3. Initial behaviour of the human proportions S, I, S_w and I_w with time (years) when p is 0.95.

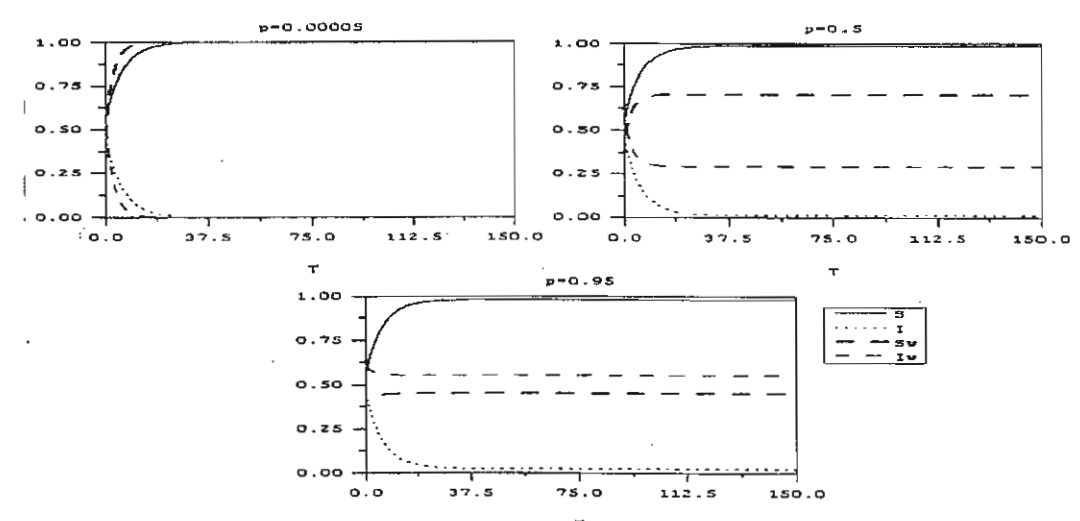


Fig 4. Long-term behaviour of the human proportions S, I, S_w and I_w with time (years) when p increases from 0.00005 to 0.5 and 0.95 respectively.

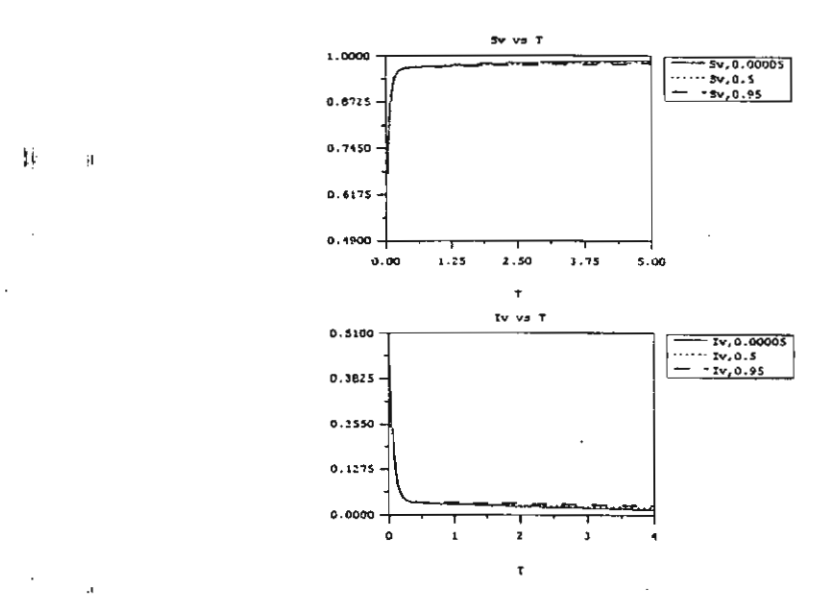


Fig 5. The behaviour of the mosquito proportions S_{ν} and I_{ν} with time (years) when p increases from 0.00005 to 0.5 and 0.95, respectively.

306

Appendix

Diving Eq.(16) by b_1 , we get

$$f(I_v^*) = I_v^{*3} + a_1 I_v^{*2} + a_2 I_v^* + a_3$$

where $a_1 = \frac{b_2}{b_1}$, $a_2 = \frac{b_3}{b_1}$, and $a_3 = \frac{b_4}{b_1}$. Since $b_1 > 0$ and $b_4 < 0$, $a_3 < 0$. We have [11]

$$\lim_{I_v^* \to \infty} f(I_v^*) = \infty \quad and \quad f(0) = a_3 < 0$$

Given the above, there is a cutting point $I_{v,0}^* \in [0,\infty)$ at which $f(I_{v,0}^*) = 0$. We, however, require at least one positive real root for I_v^* in our domain, $I_v^* \in [0,1]$. For cubic equation, we have two possibility when $f(I_v^*)$ is large where I_v^* is large $(f(I_v^*) \to \infty \text{ as } I_v^* \to \infty)$. We begin by differentiation $f(I_v^*)$. Doing this, we get

$$f'(I_n^*) = 3I_n^{*2} + 2a_1I_n^* + a_2$$

The zeros of this equation are located at the extrema of $f(I_{\nu}^{*})$ and are at

$$I_{v}^{*} = \frac{-2a_{1} \pm \sqrt{4a_{1}^{2} - 12a_{2}}}{6} = -\frac{1}{3}a_{1} \pm \frac{1}{3}\sqrt{a_{1}^{2} - 3a_{2}}$$
i.e,
$$I_{v,c_{1}}^{*} = -\frac{1}{3}a_{1} + \frac{1}{3}\sqrt{a_{1}^{2} - 3a_{2}} = -\frac{1}{3}a_{1} + \frac{1}{3}\sqrt{\Delta}$$
and
$$I_{v,c_{2}}^{*} = -\frac{1}{3}a_{1} - \frac{1}{3}\sqrt{a_{1}^{2} - 3a_{2}} = -\frac{1}{3}a_{1} - \frac{1}{3}\sqrt{\Delta}$$

case 1: all roots are positive real

Since $f(0) = a_3$, all roots would not equal to zero. In this case, both turning points are positive real so we need

$$I_{v,c_2}^* = -\frac{1}{3}a_1 - \frac{1}{3}\sqrt{a_1^2 - 3a_2} > 0$$

$$a_1 < 0$$
 and $-a_1 > \sqrt{a_1^2 - 3a_2}$ and $\Delta > 0$
 $a_1^2 > a_1^2 - 3a_2$ $a_1^2 > 3a_2$
 $a_2 > 0$

The conditions for $f(I_v^*)$ to have at least one positive real root are $a_1 < 0, a_2 > 0$ and $a_1^2 > 3a_2$.

case 2: two negative and one positive real roots

In this case, we separate the behavior of turning points into 2 cases.

case 2.1: one turning point is negative and another one is positive. We need

$$\sqrt{a_1^2-3a_2}>-a_1$$
 $a_1\geq 0$ and $-3a_2>0$ $a_2<0$

In this case, Δ is always positive since $a_2 < 0$. The conditions for $f(I_v^*)$ to have at least one positive real root are $a_1 \ge 0$ and $a_2 < 0$.

case 2.2: one turning point is negative and another turning point is negative or zero. We need

$$a_1 > 0$$
 and $a_1^2 \ge a_1^2 - 3a_2$ and $\Delta > 0$
 $a_2 \ge 0$ $a_1^2 > 3a_2$

The conditions for $f(I_v^*)$ to have at least one positive real root are $a_1 > 0, a_2 \ge 0$ and $a_1^2 > 3a_2$.

Moreover, [4] since $f(I_{v,c_2}^*) > f(0) > 0$ and $f(I_{v,c_1}^*) < 0$ so

$$\Omega^* = f(I_{v,c_1}^*)f(I_{v,c_2}^*) < 0$$

$$\Omega^* = \frac{4}{27}a_2^3 - \frac{1}{27}a_1^2a_2^2 + \frac{4}{27}a_1^3a_3 - \frac{2}{3}a_1a_2a_3 + a_3^2 < 0$$

By using
$$a_1 = \frac{b_2}{b_1}$$
, $a_2 = \frac{b_3}{b_1}$, and $a_3 = \frac{b_4}{b_1}$, Ω^* becomes

$$\Omega = \frac{4}{27}b_1b_3^3 - \frac{1}{27}b_2^2b_3^2 + \frac{4}{27}b_2^3b_4 - \frac{2}{3}b_1b_2b_3b_4 + b_1^2b_4^2.$$

Conditions (i) to (iii) in (18) are proven.

For case (iv), complex case, the possibility to get at least one positive real root is only the case for one real and two complex conjugate roots. From mathematical handbook[12], let

$$Q = \frac{3a_2 - a_1^2}{9}, \qquad R = \frac{9a_1a_2 - 27a_3 - 2a_1^3}{54}$$
$$S = \sqrt[3]{R + \sqrt{Q^3 + R^2}}, \quad T = \sqrt[3]{R - \sqrt{Q^3 + R^2}}$$

The conditions for $f(I_v^*)$ to have at least one positive real root are $Q^3 + R^2 > 0$ and $S + T > \frac{1}{3}a_1$.

$$Q^{3} + R^{2} = \frac{1}{9^{3}} (27a_{2}^{3} - 27a_{1}^{2}a_{2}^{2} + 9a_{1}^{4}a_{2} - a_{1}^{6}) + \frac{1}{54^{2}} (81a_{1}^{2}a_{2}^{2} - 486a_{1}a_{2}a_{3} - 36a_{1}^{4}a_{2} + 27^{2}a_{3}^{2} + 108a_{1}^{3}a_{3} + 4a_{1}^{6}) > 0$$

$$Q^{3} + R^{2} = \frac{4}{27}a_{2}^{3} - \frac{1}{27}a_{1}^{2}a_{2}^{2} + \frac{4}{27}a_{1}^{3}a_{3} - \frac{2}{3}a_{1}a_{2}a_{3} + a_{3}^{2} > 0$$

this is the same as Ω^* , so condition $Q^3 + R^2 > 0$ is $\Omega > 0$. By substituing $a_1 = \frac{b_2}{b_1}$, $a_2 = \frac{b_3}{b_1}$, and $a_3 = \frac{b_4}{b_1}$, the condition $S + T > \frac{1}{3}a_1$ becomes $(\frac{1}{54b_1^3}(9b_1b_2b_3 - 27b_1^2b_4 - 2b_2^3) + (\frac{\Omega}{4})^{\frac{1}{2}})^{\frac{1}{3}} + (\frac{1}{54b_1^3}(9b_1b_2b_3 - 27b_1^2b_4 - 2b_2^3) - (\frac{\Omega}{4})^{\frac{53}{2}})^{\frac{1}{3}} > \frac{b_2}{3b_1}$

References

- [1] L. Edelstein-Keshet, "Mathematical models in biology", Random House Inc., New York, 1988, 233-234.
- [2] L. Esteva and C. Vargas, Analysis of Dengue Disease Transmission Model, Math. BioSci.150(1998), 131-161.
- [3] A. Kammanee, N. Kanyamee and I.M. Tang, Basic Reproduction Number for Transmission of Plasmodium Vivax Malaria, Southeast Asian J. Trop. Med. Public Health32[4](2001), 702-706.
- [4] Q. J. A. Khan and D. Greenhalgh, Hopf bifurcation in epidemic models with a time delay, IMA J.Math.Appl.Med.Biol.16(1999), 113-142.
- [5] C. Luxemburger, M. V. Vugt, S. Jonathan, R. McGready, S. Looareesuwan, N. J. White and F. Nosten, Treatment of vivax malaria on the western border of Thailand, Trans. R. Soc. Trop. Med. Hyg. 93(1999), 433-438.
- [6] G. MacDonald, "The Epidemiology and Control of Malaria", Oxford Univ. Press, London, 1957.
- [7] P. Martents and L. Hall, Malaria on the move: Human population movement and malaria transmission, Emerging Infectious Disease 6[2](2000), 103-109.
- [8] F. E. McKenzie, Why Model Malaria?, Parasitology Today, 16[12](2000), 511-516.
- [9] R. Ross, "The Prevention of Malaria", 2nd ed., Murray, London, 1991.
- [10] R. M. Anderson and R. M. May, "Infectious diseases of humans: Dynamics and Control", Oxford Uni. Press, 1992, 375-428.
- [11] S. Ruan and J. Wei, On the zeros of a third degree exponential polynomial with applications to a delayed model for the control of testosterone secretion, IMA J.Math.Appl.Med.Biol.,18(2001), 41-52.
- [12] M. R. Spiegel, "Mathematical handbook of formulas and tables", McGraw-Hill Inc., 1990.
- [13] WHO, World malaria situation in 1994, Weekly Epidemiological Record, WHO 72[38], 1997, 285-292.
- [14] http: www.britannica.com/bcom/cb/article/310,5716,1092831+40,00.html, 2000.

Computational Mathematics and modeling, An International Conference, CMM2002, Bangkok Copyright©by East-West J. of Mathematics.

All rights of reproduction in any form reserved.



PERGAMON

Mathematical and Computer Modelling 37 (2003) 949-961

MATHEMATICAL AND COMPUTER MODELLING

www.elsevier.nl/locate/mcm

Transmission of Dengue Hemorrhagic Fever in an Age Structured Population

P. Pongsumpun

Department of Mathematics, Faculty of Science, Mahidol University Bangkok 10400, Thailand

I. M. TANG*

Department of Physics, Faculty of Science, Mahidol University Bangkok 10400, Thailand

and

Institute of Science and Technology for Research and Development Salaya Campus, Mahidol University Nakorn Pathom 71730, Thailand scimt@mahidol.ac.th

(Received May 2001; revised and accepted December 2002)

Abstract—The influence of age structure in the human population in the susceptible-infected recovered (SIR) model used to describe the transmission of Dengue hemorrhagic fever (DHF) is studied. The human population is separated into an adult class and juvenile class with the transmission of the disease being different in the two classes. Two equilibrium states are found and the condition for stability of one of these states, the disease free state, is established. The stability of the endemic state of this model is discussed. A simplified version of the model, one in which no adults become sick, is introduced. The conditions for the stability of the endemic state of this latter model are determined. Numerical calculations show that age structure in the simplified model reduces the periods of oscillations in the susceptible human population, the infected human population, and the infected mosquito population and the tightness of the spiraling into the endemic equilibrium state. © 2003 Elsevier Science Ltd. All rights reserved.

Keywords---Disease transmission, Dengue hemorrhagic fever, Age structure, SIR model.

1. INTRODUCTION

Mathematical modeling of disease transmission has a long history. In 1911, an epidemiology model for malaria transmission was developed by Ross [1]. MacDonald [2] later added a layer of biological realism to the model by providing careful interpretation and estimation of the parameter, which should go into the model. McKenzie [3] has pointed out that the utility of a model depends not as much on how well a mathematical job has been accomplished but on how well a particular question has been translated. If one is interested in disease transmission, it is imperative that

^{*}Author to whom all correspondence should be addressed.

Both authors would like to thank the Thailand Research Fund (TRF) for financial support. P. Pongsumpun would especially like to thank TRF for awarding her a Royal Golden Jubilee Ph.D. Scholarship.

^{0895-7177/03/\$ -} see front matter © 2003 Elsevier Science Ltd. All rights reserved. Typeset by AMS-TEX PII: S0895-7177(03)00111-0